Fundamentals of Vehicular Communication Networks with Vehicle Platoons

Kaushlendra Pandey, Kanaka Raju Perumalla, Abhishek K. Gupta, Harpreet S. Dhillon

***Abstract*—Vehicular platooning is a promising way to facilitate efficient movement of vehicles with a shared route. Despite its relevance, the interplay of platooning and the communication performance in the resulting vehicular network (VN) is largely unexplored. Inspired by this, we develop a comprehensive approach to statistical modeling and system-level analysis of VNs with platooned traffic. Modeling the network of roads using the by-now well-accepted Poisson line process (PLP), we place vehicles on each road according to an independent Matérn cluster process (MCP) that jointly captures randomness in the locations of platoons on the roads and vehicles within each platoon. The resulting *triply-stochastic* point process is a PLP-driven-Cox process, which we term the PLP-MCP. We first present this new point process's distribution and derive several fundamental properties essential for the resulting VN's analysis. Assuming that the cellular base-stations (BSs) are distributed as a Poisson point process (PPP), we derive the distribution of the loads served by the typical BS and the BS associated with the typical user. In deriving the latter, we also present a new approach to deriving the length distribution of a tagged chord in a Poisson Voronoi tessellation. Using the derived results, we present the rate coverage of the typical user while considering partial loading of the BSs. We also provide a comparative analysis of VNs with and without platooning of traffic.**

I. Introduction

Vehicular platooning refers to the cooperative movement of closely located vehicles having a shared route or a part of route. As part of intelligent transportation systems, platooning has enormous potential for collision avoidance among vehicles, optimization of the road capacity and fuel consumption, and reduction in pollutant gases including CO_2 emissions [1], [2]. Platooning and vehicular communication have a two way relationship. On one hand, platooning almost always ensures line-of-sight between two proximate vehicles, thereby improving the reliability of vehicle-to-vehicle (V2V) communication between them compared to independently moving vehicles [3]. Such V2V communications can help in collision and hazard warning and traffic planning [4]. Further, if one vehicle in the platoon is able to receive information via vehicle-to-infrastructure (V2I) communication, V2V communication can help relay this data to all vehicles in the platoon. On the other hand, vehicular communication is also essential in enabling platooning to reduce collision risks due to smaller intra-vehicular distance. Given the intertwined nature of these two seemingly disparate ideas, it is essential to understand their synergism, which we do here by carefully integrating platooning in the system-level analysis of vehicular networks.

K. Pandey, K. Raju Perumalla and A. K. Gupta are with IIT Kanpur, India, 208016. Email:{kpandey,pkraju,gkrabhi}@iitk.ac.in. H. S. Dhillon is with Wireless@VT, Virginia Tech, Blacksburg, VA 24061 (Email: hdhillon@vt.edu). A. K. Gupta gratefully acknowledge the support of SERB India (Grant MTR/2022/000390). H. S. Dhillon gratefully acknowledges the support of the US National Science Foundation (Grant CNS-1923807).

A. Related work

Recently, there has been a significant interest in studying different types of vehicular communication including V2V and V2I. Interested readers are advised to refer to [4], [5], and the references therein, for a comprehensive survey of this research direction. In this paper, our specific interest is on the system-level analysis of vehicular communications networks using stochastic geometry, which has attracted significant attention recently, e.g, see [6]–[10]. However, the focus of almost all of this prior work has been on conventional *non-platooning traffic scenarios* (N-PTS), where vehicles do not form platoons and hence move without any coordination with each other. For instance, in [6], [7] authors modeled the vehicular traffic on a fixed road by a 1D Poisson point process (PPP). To incorporate multiple road vehicular traffic, [8], [9] considered grid type urban roads (roads are either perpendicular, or parallel to the x-axis) modeled using the Manhattan Poisson line process (MPLP). Each road has an independent vehicular traffic distributed as 1D PPP. The authors analyzed the blockage and coverage in such networks. To include the irregularity in the layout of roads, in [10], authors suggested to model roads as Poisson line process (PLP) and vehicles as 1D PPP on each road. In this model, the combined vehicular traffic across roads forms a Cox process that can be termed PLP-PPP (*i.e.* a PLP driven PPP). A thorough investigation of various properties of PLP-PPP and its applications to vehicular communications was presented in [11].

A vehicular communication network consists of vehicular traffic overlaid with a cellular network to provide infrastructure connectivity to vehicular traffic. Such a network with N-PTS can be modeled using PLP-PPP overlaid with an independent PPP modeling the locations of BSs, owing to the mathematical tractability of these processes. In [12]–[14], authors derived the distribution of signal-to-noise-plus-interference ratio (SINR) for similar models. In [15]–[17] authors derived the SINR distribution for vehicle-to-everything (V2X) networks consisting of communications between different types of network entities, such as between BSs and vehicles, and roadside units and vehicles. Another important metric dictating the overall performance of a network is the rate distribution of the typical user. The achievable rate depends critically on the per-BS load, *i.e.* the number of vehicles present in the BS's serving region. In [15], authors derived the distribution of the per BS load and per-user rate for N-PTS. In [18], the area spectral efficiency for the N-PTS was presented. In [19], authors derived the rate coverage for cellular vehicle-to-everything (V2X) networks for N-PTS.

Although past works have analyzed the vehicular communication network with N-PTS, analytical tools have not

been fully explored yet to study the *platooned vehicular traffic scenario* (PTS) and its impact on the performance of a vehicular communication. Consequently, there is limited work focusing on the analysis of PTS [20]–[22]. For example, in [20], authors considered a single road vehicular traffic consisting of independent vehicles and platoons, both modeled as points of 1D PPP and derived the probability that vehicles can communicate with each other. In [21], authors considered platooned traffic on a single road with BSs deployed on the side of the road and derived approximate coverage. In [22], authors considered platooned traffic on a single road with road side BSs and performed a joint communication and control analysis to study the stability and delay in the network. One main limitation of the above works is that they considered vehicular traffic on a single road. In practice, the "support" of a vehicular network is a complicated layout of roads that needs to be accounted for and is one of the key reasons for the popularity of the PLP-based models. A vehicular traffic on such a road network is further complicated by the randomness in the number and locations of platoons and locations of vehicles in each platoon. As indicated above, the wireless performance of a vehicular user depends critically on the per BS load which has not been analyzed in the previous work for PTS. Overall, the interplay of platooning and the vehicular network performance is largely unexplored from the perspective of rigorous system-level analysis. This paper attempts to bridge this gap. In particular, we try to explore how we can model a complete vehicular communication network consisting of a 2D network of BSs and the vehicles moving in platoons and analyze the performance of this network in terms of load and rate distribution.

B. Contributions

In this paper, we develop an analytical framework for a vehicular communication system (in particular, a V2I scenario) with platooned traffic. We propose a novel point process for modeling the platoon movement of vehicles. We then examine the impact of platooning on V2I communication by observing the load that appears on the infrastructure network. We present a comparative study of the rate coverage for PTS and N-PTS. The important contributions of this paper are listed below.

1) We propose a novel point process termed PLP-MCP for the modeling and analysis of the platooned movement of the vehicles. It is a Cox process driven by the PLP that captures three layers of randomness: (i) irregularity in the road layout, (ii) randomness in the locations of the platoons, and (iii) randomness in the locations of vehicles within a platoon. In this sense, this process can be thought of as a *triply-stochastic* process that generalizes *doubly-stochastic* PLP-PPP used in the literature [11]. We present its distribution and key properties essential for the analysis of the vehicular traffic.
2) We then present an analytical framework to characterize the performance of the typical user in a V2I communication network consisting of BSs and platooned traffic.
3) We derive the load distribution for the typical and the tagged BSs along with the means and variances. Here, tagged BS is the BS that serves the typical user. As a key intermediate result, we derive a new expression for the distribution of the tagged chord in the Voronoi cell of the tagged BS.
4) Using the derived results, we present the rate coverage of the typical user while considering the partial loading of BSs. We perform a comparative analysis of load distribution and rate coverage of communication systems with platooned movement with non-platooned movement to understand the impact of vehicular platooning.

Fig. 1 summarizes the main results of the paper along with their mutual relationship.

TABLE I: Notation Table

Parameter	Definition
$\boldsymbol{x}, \lvert\boldsymbol{x}\rvert$	A vector $\boldsymbol{x}$ in $\mathbb{R}$ with its norm as $\lvert\boldsymbol{x}\rvert$.
$\mathbf{x}, \lVert x\rVert$	A vector $\mathbf{x}$ in $\mathbb{R}^2$ with its norm as $\lVert\mathbf{x}\rVert$.
$\mathsf{B}_n(\boldsymbol{x}, r)$	nD Ball of radius r centred at location $\boldsymbol{x}$.
A and $\lvert\mathsf{A}\rvert$	Set A with its Lebesgue measure as $\lvert\mathsf{A}\rvert$.
$\mathcal{P}_X(\cdot)$, $\mathbb{E}[X]$ and $\mathrm{Var}[X]$	The PGF, expected value and variance of RV X.
o	The origin $(0, 0)$.
$\ell = \mathsf{L}(\rho, \phi)$	A line in $\mathbb{R}^2$ in Hesse normal form, *i.e.* the normal segment from origin to the line is of length ρ and makes angle ϕ with respect to the x-axis.
$(\rho\cos\phi, \rho\sin\phi)$	Nearest point on the line $\mathsf{L}(\rho, \phi)$ from the origin termed the base.
$\mathcal{A}_1(a, b, x)$	Length of the intersection of two 1D balls $\mathsf{B}_1(\mathrm{o}, a)$ and $\mathsf{B}_1(\boldsymbol{x}, b)$.
$\mathsf{b}(\cdot)$	Bell's polynomial [23].
$\Psi^!$ and $\Psi^{!\mathrm{o}}$	The Palm and the reduced Palm version of the point process Ψ.
$\Psi(\mathsf{C})$	Number of points of point process Ψ falling inside set C.
$\beta(r, a)$	$2\min(r, a)$.
$\widetilde{(\cdot)}$	Approximated variable.
$\widehat{X}$	Denotes the RV X under the reduced Palm version of the point process.
$A \overset{(d)}{=} B$	The RV A and RV B have the same distribution.
Ψ_{m} and λ_{m}	PLP-MCP with density λ_{m}.
$S(r)$	Number of points of Ψ_{m} falling in ball $\mathsf{B}_2(\mathrm{o}, r)$.
$\widehat{S}(r)$	Number of points of Ψ_{m} falling in ball $\mathsf{B}_2(\mathrm{o}, r)$ conditioned $\mathrm{o} \in \Psi_{\mathrm{m}}$.
$\widetilde{S}_{\mathrm{m}}$ and $\widetilde{M}_{\mathrm{m}}$	Approximated load on the typical and tagged cell respectively in PTS.
$\widetilde{S}_{\mathrm{p}}$ and $\widetilde{M}_{\mathrm{p}}$	Approximated load on the typical and tagged cell respectively in ITS.

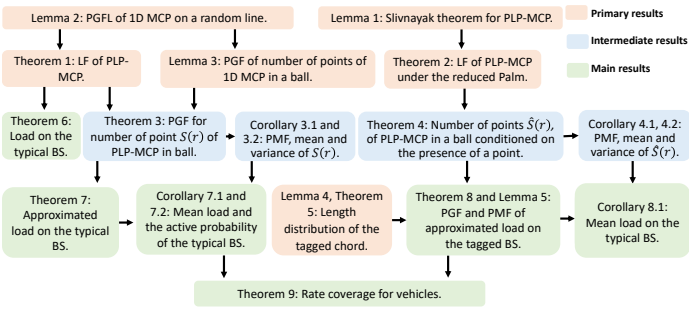

Fig. 1: Illustration showing relationship between the derived results.

II. Modeling of Platooned Vehicles using PLP-MCP

In vehicular networks, the randomness caused by the orientation of roads and the positions of vehicles can be modeled using the doubly stochastic process PLP-PPP. However, this model may not be suitable for modeling the randomness

introduced by factors such as the location of platoons, the position of vehicles within a platoon, and the size of platoons. Therefore, to model such a scenario, a triply stochastic process is necessary, which can effectively integrate these sources of randomness while preserving the mathematical tractability of the PP. In this paper, we introduce a novel point process PLP-MCP to model platooned vehicles on a network on roads. The system model is as follows.

A. Road network

The network of roads can be modeled by a PLP $\Phi_{\rm L} = \{\ell_1, \ell_2, \cdots\}$ with density $\lambda_{\rm L}$ where ℓ_i denotes the ith road [11]. The line $\ell = \mathsf{L}(\rho, \phi)$ can also be represented as an element (ρ, ϕ) of the set $\mathbf{C}^* \equiv \mathbb{R} \times [0, \pi)$. We term the element (ρ, ϕ) as L-atom and $\mathbf{C}^*$ as L-space. Further, The point (ρ, ϕ) in $\mathbf{C}^*$ is corresponding to $(\rho\cos\phi, \rho\sin\phi) \in \mathbb{R}^2$, where ρ denotes the distance of the point $(\rho\cos\phi, \rho\sin\phi)$ from origin and ϕ represents the angle between the positive x-axis of $\mathbb{R}^2$ and the line joining the point with origin $\mathrm{o} \equiv (0,0)$. Therefore the ith line $\ell_i \in \Phi_{\rm L}$ can be denoted by the L-atom $a_i = (\rho_{\ell_i}, \phi_{\ell_i})$ in the L-space $\mathbf{C}^*$. The L-atoms a_i's form a PPP in $\mathbf{C}^*$ with density $\lambda_{\rm L}$. This means that the mean number of lines hitting a convex body K with perimeter $L(\mathsf{K})$ is $\lambda_{\rm L} L(\mathsf{K})$ [11]. The validity of modeling roads via a PLP was studied and verified in the past work, e.g. [24]–[26]. The analysis of this paper can be extended to include scenarios with different types of roads including the Manhattan line process.

B. Platooned vehicles

For each road ℓ_i, vehicular platoons can be seen as the clusters of vehicles in a finite spread. Cluster processes (with MCP being a special case) offer a natural way of modeling platooned traffic, wherein vehicles in the same platoon are close by (hence clustered). The MCP was a natural cluster process to choose because of its bounded support and tractability. We model the vehicles on the road ℓ_i by an independent MCP Ψ_i with parent PP density $\lambda_{\rm P}$, mean number of points per cluster m and cluster radius a. In particular, the platoon centers are distributed as the parent PP $\overline{\Psi}_i^{(\rm p)}$. For a platoon centered at $\boldsymbol{x}_{j,i} \in \overline{\Psi}_i^{(\rm p)}$, the constituent vehicles are distributed as the PPP $\overline{\Omega}_{\boldsymbol{x}_{j,i}}$ in $a-$neighborhood of it. Let $\mu_{\rm m}$ denote the per-road vehicular density *i.e.* $\mu_{\rm m} = m\lambda_{\rm P}$.

The locations of all vehicles form a new PP, which we term as PLP-MCP. It can be formally defined as follows.

Definition 1 (PLP-MCP)**.** *Let $\Phi_{\rm L} = \{\ell_1, \ell_2, \cdots\}$ be a PLP with density $\lambda_{\rm L}$ with the ith line $\ell_i = \mathsf{L}(\rho_{\ell_i}, \phi_{\ell_i})$. Let $\{\overline{\Psi}_i\}$ be a set of independent and identically distributed 1D MCP in $\mathbb{R}$ with parameter $(m, \lambda_{\rm P}, a)$ such that*

$$\overline{\Psi}_i = \bigcup\nolimits_{\boldsymbol{x}_{j,i} \in \overline{\Psi}_i^{(\rm p)}} \overline{\Omega}_{\boldsymbol{x}_{j,i}},$$

where $\overline{\Psi}_i^{(\rm p)}$ is a PPP with density $\lambda_{\rm P}$. $\overline{\Psi}_i^{(\rm p)}$ is called the parent point process of $\overline{\Psi}_i$ as it consists of parent points $\boldsymbol{x}_{j,i} \in \mathbb{R}$. Further, $\overline{\Omega}_{\boldsymbol{x}_{j,i}}$ denotes the daughter PP of $\boldsymbol{x}_{j,i}$ and is a PPP with density $\lambda_{\rm d} = m/(2a)$ in $\mathsf{B}_1(\boldsymbol{x}_{j,i}, a)$. We assign ith MCP $\overline{\Psi}_i$ to the ith line ℓ_i and transform the points of $\overline{\Psi}_i$ to be on the line to get

$$\begin{aligned}\Psi_{\ell_i} &= \bigcup\nolimits_{\boldsymbol{x}_{j,i} \in \overline{\Psi}_i^{(\rm p)}} \{\mathbf{z}_{k,j,i} = f_{\ell_i}(\overline{\boldsymbol{z}}_{k,j,i}) : \overline{\boldsymbol{z}}_{k,j,i} \in \overline{\Omega}_{\boldsymbol{x}_{j,i}}\} \\ &= \bigcup\nolimits_{\boldsymbol{x}_{j,i} \in \overline{\Psi}_i^{(\rm p)}} \Omega_{\boldsymbol{x}_{j,i}}, \end{aligned} \tag{1}$$

where $\Omega_{\boldsymbol{x}_{j,i}}$ represents $\overline{\Omega}_{\boldsymbol{x}_{j,i}}$ transformed on line ℓ_i and $f_\ell()$ denotes the transformation of $\mathsf{L}(0,0)$ to the line $\ell = \mathsf{L}(\rho_\ell, \phi_\ell)$ given as

$$f_\ell(\overline{\boldsymbol{x}}) = (\rho_\ell \cos\phi_\ell + \overline{\boldsymbol{x}}\sin\phi_\ell, \rho_\ell \sin\phi_\ell - \overline{\boldsymbol{x}}\cos\phi_\ell)\,. \tag{2}$$

*This means that if $\overline{\boldsymbol{x}}$ is a scalar quantity denoting the location of a point in the line ℓ relative to its base, its 2D coordinates (*i.e. *absolute location in $\mathbb{R}^2$) are given as $\mathbf{x} = f_\ell(\overline{\boldsymbol{x}})$. Now, a PLP-MCP $\Psi_{\rm m}$ is defined as the union of all Ψ_{ℓ_i}'s* i.e.

$$\Psi_{\rm m} = \bigcup\nolimits_{\ell_i \in \Phi_{\rm L}} \Psi_{\ell_i}, \tag{3}$$

and includes all the points located on every line of $\Phi_{\rm L}$.

Hence, the platoon vehicular traffic can be modeled using points of the proposed PLP-MCP $\Psi_{\rm m}$. The absolute location of k-th vehicles in jth platoon of ith road is given as $\mathbf{z}_{k,j,i}$. As the suggested PP allows for varying the platoon parameter, and has the advantage of mathematical tractability, we expect that the main results presented in the paper will show similar trends when compared to slightly different variants of this model (capturing different distributions of the roads and vehicles on them).

C. Properties of PLP-MCP

We now describe some key properties of the PLP-MCP that are helpful in the analysis of vehicular communication.

1) *Stationarity:* The PLP-MCP $\Psi_{\rm m}$ is a stationary PP. The stationarity of $\Psi_{\rm m}$ follows from the stationarity of PLP and 1D MCP.
2) *Density:* The density $\lambda_{\rm m}$ of $\Psi_{\rm m}$ is $m\lambda_{\rm P}\lambda_{\rm L}\,\pi$. The density of $\Psi_{\rm m}$ can be derived by counting the mean number of points in a unit area using the Campbell's theorem [27].
3) It is a Cox process driven by a PLP.

For a stationary PP, we can take the typical point at the origin [27]. Further, if the typical point is located at the origin, the tagged line $\ell_{\rm o}$ passes through the origin.

III. Characterization of PLP-MCP

In this section, we will present several key properties of the proposed PLP-MCP.

A. Extended Slivnyak Theorem

Since PLP-MCP is derived from PLP (which is a PPP in L-space), Slivnyak theorem can be extended to describe the conditional distribution of PLP-MCP. Even though this extension is not overly challenging, we decided to present it separately upfront so that we can easily refer to it throughout the paper rather than repeating this same argument everywhere.

Lemma 1. *(Extended Slivnyak Theorem.) Conditioned on the typical point $\mathbf{z}_{\rm o}$, the distribution of the rest of the PLP-MCP $\Psi_{\rm m}$ is equal to the distribution of an independent copy of $\Psi_{\rm m}$ superposed with an independent copy of the MCP $\Psi_{\ell_{\rm o}}$ on the tagged line $\ell_{\rm o}$ and an independent copy of the cluster PPP $\Omega_{\boldsymbol{x}_{\rm o}}$ (which is $\overline{\Omega}_{\boldsymbol{x}_{\rm o}}$ transformed on $\ell_{\rm o}$). Here, $\boldsymbol{x}_{\rm o}$ denotes the*

parent point of the typical point and distributed uniformly in the 1D $a-$neighborhood of $\boldsymbol{z}_{\mathrm{o}} = f_{\ell_{\mathrm{o}}}^{-1}(\mathbf{z}_{\mathrm{o}})$. In other words,

$$\Psi_{\mathrm{m}}^{!}|(\mathbf{z}_{\mathrm{o}} \in \Psi_{\mathrm{m}}) \overset{(d)}{=} \Psi_{\mathrm{m}} \cup \Psi_{\ell_{\mathrm{o}}} \cup \Omega_{\boldsymbol{x}_{\mathrm{o}}}. \tag{4}$$

Proof. Conditioning on the occurrence of the typical point fixes the tagged parent point $\boldsymbol{x}_{\mathrm{o}}$ and the tagged line ℓ_{o}. Since PLP Φ_{L} is a PPP in L-space, conditioned on ℓ_{o}, Φ_{L} is equivalent to the union of ℓ_{o} and an independent copy of Φ_{L} (which generates an independent copy of Ψ_{m}). Now, $\overline{\Psi}_{\ell_{\mathrm{o}}}^{(\mathrm{p})}$ is also a PPP containing $\boldsymbol{x}_{\mathrm{o}}$, hence, conditioned on $\boldsymbol{x}_{\mathrm{o}}$, it is equivalent to the union of $\boldsymbol{x}_{\mathrm{o}}$ and an independent copy of $\overline{\Psi}_{\ell_{\mathrm{o}}}^{(\mathrm{p})}$ which generates $\Psi_{\ell_{\mathrm{o}}}$. Again, $\Omega_{\boldsymbol{x}_{\mathrm{o}}}$ is a PPP, hence, conditioned on $\mathbf{z}_{\mathrm{o}}$, $\Omega_{\boldsymbol{x}_{\mathrm{o}}}$ is equivalent to the union of $\boldsymbol{x_0}$ and an independent copy of $\Omega_{\boldsymbol{x}_{\mathrm{o}}}$. □

B. Laplace functional

Since the distribution of a PP is completely characterized by its Laplace functional (LF), we now derive the LF for PLP-MCP. We will first require the PGFL of the MCP Ψ_{ℓ_i} transformed on the line ℓ_i which is given in Lemma 2. Let there be a function $v : \mathbb{R}^2 \to [0,\, 1]$.

Lemma 2. *The PGFL of Ψ_ℓ on road ℓ is given as*

$$\mathcal{G}_{\Psi_\ell,\ell}\,(v) = \exp\left(-\lambda_{\mathrm{P}} \int_{\mathbb{R}} \left(1 - \mathcal{H}_{\boldsymbol{x},\ell}(v)\right) \mathrm{d}\boldsymbol{x}\right), \tag{5}$$

*where $\mathcal{H}_{\boldsymbol{x},\ell}(v) = \exp\left(-\lambda_{\mathrm{d}} \int_{\mathsf{B}_1(\mathrm{o},a)} \left(1 - (v \circ f_\ell)\,(\boldsymbol{x}+\boldsymbol{y})\right) \mathrm{d}\boldsymbol{y}\right)$. Under reduced Palm (*i.e. *conditioned on occurrence of a point at $\mathbf{z}_{\mathrm{o}}$ excluding $\mathbf{z}_{\mathrm{o}}$), PGFL of Ψ_ℓ on road ℓ is*

$$\mathcal{G}_{\Psi_\ell,\ell}^{!\mathbf{z}_{\mathrm{o}}}(v) = \frac{\mathcal{G}_{\Psi_\ell,\ell}\,(v)}{2a} \int_{\mathsf{B}_1(f_\ell^{-1}(\mathbf{z}_{\mathrm{o}}),a)} \mathcal{H}_{-\boldsymbol{x}_{\mathrm{o}},\ell}(v) \mathrm{d}\boldsymbol{x}_{\mathrm{o}}. \tag{6}$$

Here, $\boldsymbol{x}_{\mathrm{o}}$ denotes the untransformed center of the parent cluster of $\mathbf{z}_{\mathrm{o}}$.

The following remark explains how the LF and its Palm version enable us to examine the platooned vehicular networks from two different perspectives.

Remark 1. *In the uplink analysis of a wireless network, when the received power attenuates in accordance with the distance-based path loss model, the LF may be utilized to determine the LF of total interference from the vehicles seen by any point in $\mathbb{R}^2$ plane.*

Moreover, if we want to capture the interference seen by any vehicle from all the other vehicles in V2V communication, the Palm version of the LF may be used to get the LF of interference. We now derive the LF for PLP-MCP which is given in the following two Theorems. See Appendix A for the proofs.

Theorem 1. *The LF for Ψ_{m} is given as*

$$\mathcal{L}_{\Psi_{\mathrm{m}}}(v) = \mathbb{E}\left[e^{-\sum_{\mathbf{z}\in\Psi_{\mathrm{m}}} v(\mathbf{z})}\right]$$
$$= \exp\left(-\lambda_{\mathrm{L}} \int_{\mathbb{R}} \int_0^{\pi} \left(1 - \mathcal{G}_{\Psi_{\mathsf{L}(\rho,\phi)},\mathsf{L}(\rho,\phi)}\left(e^{-v}\right)\right) \mathrm{d}\rho\, \mathrm{d}\phi\right), \tag{7}$$

where $\mathcal{G}_{\Psi_\ell,\ell}\,(v)$ is given in (5)*.*

Theorem 2. *The LF for Ψ_{m} under the reduced Palm distribution is*

$$\mathcal{L}_{\Psi_{\mathrm{m}}}^{!\mathrm{o}}(v) = \mathbb{E}^{!\mathrm{o}}\left[e^{-\sum_{\mathbf{z}\in\Psi_{\mathrm{m}}} v(\mathbf{z})}\right]$$
$$= \mathcal{L}_{\Psi_{\mathrm{m}}}(v) \int_0^{\pi} \pi^{-1} \mathcal{G}^{!\mathrm{o}}{}_{\Psi_{\mathsf{L}(0,\phi)},\mathsf{L}(0,\phi)}(e^{-v})\, \mathrm{d}\phi. \tag{8}$$

C. Distribution of number of points (vehicles) of Ψ_{m} in a set

The PP Ψ_{m} can also be characterized by the distribution of the number of its points in a set which is crucial in computing the load distribution in vehicular communication network which will be discussed in the next section. To derive this distribution, we will first require the PGF of the number N_ℓ of points of the MCP Ψ_ℓ on the line ℓ which is given in Lemma 3.

Lemma 3. *Let Ψ_ℓ denotes a 1D MCP on line $\ell = \mathsf{L}\,(\rho, \phi)$. The PGF for the number N_ℓ of points of Ψ_ℓ falling inside $\mathsf{B}_2(\mathrm{o}, r)$ is*

$$\mathcal{P}_{N_\ell}(s,r) = \exp\left(g(s, \sqrt{r^2 - \rho^2})\right) \tag{9}$$

$$\textit{where, } g(s,t) = 2\lambda_{\mathrm{P}} \Big[|t-a|\, e^{\lambda_{\mathrm{d}}\beta(t)(s-1)} - (t+a) + (e^{\lambda_{\mathrm{d}}(s-1)\beta(t)} - 1)/(\lambda_{\mathrm{d}}(s-1))\Big]. \tag{10}$$

Note that $\rho = 0$ gives the PGF of N_ℓ when the line passes through the origin with an angle of ϕ. The k-th derivative of $g(s,t)$ with respect to s is given as

$$g^{(k)}(s,t) = 2\lambda_{\mathrm{P}} \left[(\lambda_{\mathrm{d}}\beta(t))^k |t-a| e^{(s-1)\lambda_{\mathrm{d}}\beta(t)} + \frac{1}{\lambda_{\mathrm{d}}} \left(\sum_{j=0}^{k} \binom{k}{j} \frac{j!(-1)^j}{(s-1)^{j+1}} (\lambda_{\mathrm{d}}\beta(t))^{k-j} e^{(s-1)\lambda_{\mathrm{d}}\beta(t)} - \frac{k!(-1)^k}{(s-1)^{k+1}}\right)\right]. \tag{11}$$

To derive the mean and variance, we need $\lim_{s\to 1} g^{(k)}(s,t)$. Let $\lim_{s\to 1} g^{(k)}(s,t) = \kappa(t,k)$ which is given as

$$\lim_{s\to 1} g^{(k)}(s,t) = \kappa(t,k) = 2\lambda_{\mathrm{P}} \left(\lambda_{\mathrm{d}}\beta(t)\right)^k \left[|t-a| + \frac{\beta(t)}{(k+1)}\right]. \tag{12}$$

We now present the distribution of the number $S(r)$ of points of Ψ_{m} in a 2D ball of radius r *i.e.* $S(r) = \Psi_{\mathrm{m}}(\mathsf{B}_2(\mathrm{o}, r))$ in terms of its PGF and PMF along with its mean and variance. The PGF of $S(r)$ may be used to calculate the distribution of contact distance, which is defined as the distance between the closest Ψ_{m} point and any randomly chosen point in $\mathbb{R}^2$. For the approximated load distribution study, we will directly use the formulas stated in Theorem 3 and Corollary 3.1. The mean and variance of $S(r)$ calculated in Corollary 3.2 may be used directly to calculate the approximated mean load and variance of the load distribution on the BS. Note that the PMF, the mean and the variance of a discrete RV X can be computed from its PGF using the following relation

$$p_X(k) = \mathbb{P}[X = k] = \frac{1}{k!}\left[\mathcal{P}_X^{(k)}(s,r)\right]_{s=0} \quad \forall k \tag{13}$$

$$\mathbb{E}[X] = \left[\mathcal{P}_X^{(1)}(s)\right]_{s=1}, \tag{14}$$

$$\mathrm{Var}[X] = \left[\mathcal{P}_X^{(2)}(s)\right]_{s=1} + \mathbb{E}\,[X] - (\mathbb{E}\,[X])^2. \tag{15}$$

Therefore, we get the following result. See Appendix B for the proofs of the following results.

Theorem 3. *The PGF of the number $S(r)$ of points of Ψ_{m} inside $\mathsf{B}_2(\mathrm{o},r)$ is*

$$\mathcal{P}_{S(r)}(s)=\exp\left(-2\pi\lambda_{\mathrm{L}}\left(r-\int_0^r\frac{\exp(g(s,t))t}{\sqrt{r^2-t^2}}\mathrm{d}t\right)\right), \quad (16)$$

where $g(s,t)$ is given in (10)*.*

Corollary 3.1. *The PMF of $S(r)$ is given by*

$$\mathbb{P}[S(r)=n]=\frac{1}{n!}\mathcal{P}_{S(r)}(0)\ \mathsf{b}\left(f_{\mathrm{m}}^{(1)}(r),\cdots,f_{\mathrm{m}}^{(n)}(r)\right), \quad (17)$$

with $f_{\mathrm{m}}^{(k)}(r)=$

$$2\pi\lambda_{\mathrm{L}}\int_0^r\frac{\exp\left(g(0,t)\right)}{\sqrt{r^2-t^2}}\mathsf{b}\left(g^{(1)}(0,t),\cdots,g^{(k)}(0,t)\right)t\mathrm{d}t, \quad (18)$$

and $g^{(k)}(0,t)$ can be evaluated from (11)*.*

Corollary 3.2. *The mean and variance of $S(r)$ is*

$$\mathbb{E}\left[S(r)\right]=\left[\mathcal{P}_{S(r)}^{(1)}(s)\right]_{s=1}=\lambda_{\mathrm{m}}\pi r^2, \quad (19)$$

$$\mathrm{Var}(S(r))=\begin{cases}\lambda_{\mathrm{m}}\pi r^2+2\pi\lambda_{\mathrm{L}}\left[\frac{32}{3}\left(a\lambda_{\mathrm{P}}\lambda_{\mathrm{d}}\right)^2r^3\right.\\ \left.+8\lambda_{\mathrm{P}}\lambda_{\mathrm{d}}^2\left(\frac{2}{3}ar^3-\frac{1}{16}\pi r^4\right)\right], & a>r\\ \lambda_{\mathrm{m}}\pi r^2+\left(\frac{8\lambda_{\mathrm{P}}\lambda_{\mathrm{d}}a}{3}\right)^2\pi\lambda_{\mathrm{L}}r^3\\ +4\pi\lambda_{\mathrm{L}}\lambda_{\mathrm{P}}\lambda_{\mathrm{d}}^2\left(r^3\left(\frac{8a}{3}-\frac{\pi r}{4}\right)\right.\\ +\sqrt{r^2-a^2}\left(-\frac{a^3}{3}-\frac{13ar^2}{6}\right)+\left(2a^2r^2+\frac{r^4}{2}\right)\\ \left.\times\sin^{-1}\left(\frac{\sqrt{r^2-a^2}}{r}\right)\right). & a<r,\end{cases} \quad (20)$$

D. Distribution of number of points of Ψ_{m} in a set under Palm distribution

We also present the distribution of number of points inside a set under Palm distribution (conditioned on occurrence of a point at the origin *i.e.* $\mathrm{o}\in\Psi_{\mathrm{m}}$). Similar to previous section, we can compute the PMF and the mean of $\widehat{S}(r)$ from its PGF. The PGF of $\widehat{S}(r)$ can be used directly to derive the CDF of NND which is defined as the distance of the nearest point from any typical point of Ψ_{m}. Further, it is crucial to comprehend the distribution of vehicles around the typical vehicle in a platooned vehicular network where the vehicles continuously broadcast information about their speed and location. Using Theorem 4, we can easily derive performance metrics such as the mean number of vehicles falling within the typical vehicle's broadcast radius. See Appendix C for the proof of the following results.

Theorem 4. *The PGF of the number $\widehat{S}(r)$ of points of $\Psi_{\mathrm{m}}\setminus\{\mathrm{o}\}$ conditioned on $\mathrm{o}\in\Psi_{\mathrm{m}}$, falling inside $\mathsf{B}_2(\mathrm{o},r)$ is*

$$\mathcal{P}_{\widehat{S}(r)}(s)=\mathcal{P}_{S(r)}(s)\frac{e^{g(s,r)}}{a}\int_0^a e^{(s-1)\lambda_{\mathrm{d}}\mathcal{A}_1(r,a,x)}\mathrm{d}x, \quad (21)$$

where $\mathcal{P}_{S(r)}(s)$ is presented in Theorem 3, $g(s,\cdot)$ is given in (10) *and $\mathcal{A}_1(a,b,x)$ is [28]*

$$\mathcal{A}_1(a,b,x)=\begin{cases}2\min(a,b), & \text{if } 0\le x\le|a-b|\\ a+b-x, & \text{if } |a-b|<x\le a+b.\end{cases} \quad (22)$$

Corollary 4.1. *The PMF of $\widehat{S}(r)$ is*

$$\mathbb{P}\left[\widehat{S}(r)=n\right]=$$

$$\frac{1}{n!}\sum_{k_1+k_2+k_3=n}\left[\binom{n}{k_1,k_2,k_3}\prod\nolimits_{1\le t\le 3}f_t^{(k_t)}(0,r)\right], \quad (23)$$

where $f_1^{(k)}(0,r)=\mathcal{P}_{S(r)}^{(k)}(0)$

$$=\mathcal{P}_{S(r)}(0)\ \mathsf{b}\left(f_{\mathrm{m}}^{(1)}(0,r),\cdots,f_{\mathrm{m}}^{(k)}(0,r)\right) \quad (24)$$

$$f_2^{(k)}(0,r)=e^{g(0,r)}\ \mathsf{b}\left(g^{(1)}(0,r)...g^{(k)}(0,r)\right) \quad (25)$$

$$f_3^{(k)}(0,r)=\int_0^a\left(\lambda_{\mathrm{d}}\mathcal{A}_1(r,a,x)\right)^k a^{-1}e^{-\lambda_{\mathrm{d}}\mathcal{A}_1(r,a,x)}\mathrm{d}x, \quad (26)$$

with $g(\cdot)$ is given in (10) *and $f_{\mathrm{m}}^{(k)}(0,r)$ in* (18)*.*

Corollary 4.2. *The expected value of $\widehat{S}(r)$ is $\mathbb{E}\left[\widehat{S}(r)\right]=\lambda_{\mathrm{m}}\pi r^2+2\lambda_{\mathrm{P}}mr+\lambda_{\mathrm{d}}\left(2r-r^2/(2a)\right)$.*

In this section, we have presented several key properties of PLP-MCP. These properties are PGFL, density, LF under the reduced palm distribution, the PGF (and PMF) for the number of points falling inside ball $\mathsf{B}_2(\mathrm{o},r)$ both under normal and Palm distributions. In the next section, we introduce the vehicular communication network providing connectivity to the platooned vehicles and present the distribution for the length of the typical and the tagged chord of the typical cell, and 0-cell respectively of a homogeneous 2D PPP. These distributions are essential to derive the load distribution on the typical and tagged BS.

IV. Vehicular Communication Network

The complete vehicular communication network consists of vehicular traffic (as defined in Section II) overlaid with the BSs forming a cellular network (See Fig. 2). The role of the cellular BS network is to provide cellular V2I connectivity to vehicular users. We model the locations of BSs as a 2D PPP $\Phi_{\mathrm{b}}\equiv\left\{\mathbf{y}_i,:\mathbf{y}_i\in\mathbb{R}^2,\,\forall i\in\mathbb{N}\right\}$ with density λ_{b} [27]. Each BS transmits with the same power. The user association is based on the maximum average received power from the BSs and each user is connected to its nearest BS. Furthermore, we assume that the BS without any associated user will stay silent and not create interference. The active BSs point process $\Phi_{\mathrm{b}}^{'}$ can be approximated as PPP with the active BS density $p_{\mathrm{on}}\lambda_{\mathrm{b}}$ where p_{on} is the *active probability* [29]. Now, in order to study the average property seen by the points of a stationary PP, a general methodology is to hold a point of the PP at the origin and average the property seen from this point over all realizations. Such a point is termed the typical point of the PP. It can be intuitively seen as a point selected from the PP without any selection bias. It captures the ensemble average in the same way as one would get a spatial average in a large realization of a PP by observing the quantity of interest at each point and then averaging over all the points. Here, we consider the typical vehicle defined as the typical point in Ψ_{m}. We consider the typical vehicle to be at the origin, owing to the stationarity of Ψ_{m}. Now, the signal to interference ratio (SIR) at the typical vehicle is given by

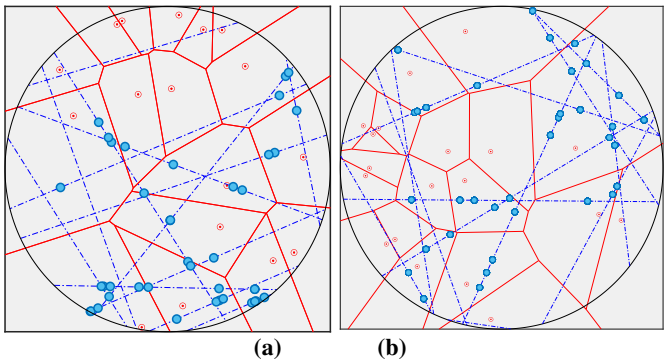

Fig. 2: (a) An illustration showing the complete vehicular network with platooned vehicles. The vehicles (shown as blue circles) on the road (shown as dotted line). Each BS (presented by points) has an associated serving area (bounded by the lines). As shown in the figure, the cluster movement of vehicles may assist them in connecting with the nearby vehicles for data, and content sharing. (b) A vehicular communication network with independently moving vehicles is shown for comparison.

$$\mathtt{SIR} = \frac{h_0 R^{-\alpha}}{\sum_{\mathbf{y}\in\Phi_{\mathrm{b}}'} h_{\mathbf{y}} \|\mathbf{y}\|^{-\alpha}}, \tag{27}$$

where R denotes the distance of the nearest BS, α is path loss exponent, h_0 denotes the fading gain of the typical receiver link and $h_{\mathbf{y}}$ denotes the fading gains of the rest of the links. Further, we have assumed that the fading coefficients $h_{(.)}$ are exponentially distributed with unit mean.

Due to the considered association policy, the serving region of each BS is its Voronoi cell. For a BS located at $\mathbf{y}$, its Voronoi cell $\mathsf{V}_{\mathbf{y}}$ is $\mathsf{V}_{\mathbf{y}} = \left\{\mathbf{x}\in\mathbb{R}^2 : \mathbf{y} = \arg\min_{\mathbf{y}_i\in\Phi_{\mathrm{b}}} \|\mathbf{x}-\mathbf{y}_i\|\right\}$. Let X_{b} denote the union of Voronoi edges. The users connected to any BS constitute the load on that BS. The **typical BS** is the typical point of the BS PP Φ_{b}. The Voronoi cell associated with the typical BS is known as **the typical Voronoi cell denoted as** V_{t}**.** Its area $|\mathsf{V}_{\mathrm{t}}|$ is empirically distributed as a generalized gamma RV [30]. The PDF of the generalized Gamma distribution with parameters a_1, b_1, c_1 is denoted by

$$\tilde{g}_X(x; a_1, b_1, c_1) = a_1 b_1^{c_1/a_1} \left(\Gamma\left(c_1/a_1\right)\right)^{-1} x^{c_1-1} e^{-b_1 x^{a_1}}. \tag{28}$$

For the typical Voronoi cell, the parameters are $a_1 = 1.07950, b_1 = 3.03226$ and $c_1 = 3.31122$ [31]. Hence, its PDF is

$$g_{|V_{\mathrm{t}}|}(v_{\mathrm{t}}) = \lambda_{\mathrm{b}} \tilde{g}_X\left(\lambda_{\mathrm{b}} v_{\mathrm{t}}; a_1, b_1, c_1\right). \tag{29}$$

Similarly, the perimeter of $Z = L(V_{\mathrm{t}})$ has the empirical distribution [30]

$$p_Z(z) = \frac{\sqrt{\lambda_{\mathrm{b}}}}{4}\, \tilde{g}_X\left(\frac{\sqrt{\lambda_{\mathrm{b}}} z}{4}; 2.33609, 2.97006, 7.58806\right). \tag{30}$$

A line ℓ_{o} of Φ_{L} that passes through the typical point of PP (Ψ_{m}) is termed as *the tagged line*. Here, $\ell_{\mathrm{o}} = \mathsf{L}(0, \phi)$ with $\rho = 0$ and ϕ is a uniform RV between 0 to π. Now, let us consider the typical vehicle at the origin. The BS which is associated with the typical vehicle is termed **the tagged BS**. The Voronoi cell of the tagged BS is termed as **the zero cell or the tagged cell** [32] given as $\mathsf{V}_{\mathrm{o}} = \left\{\mathbf{x}\in\mathbb{R}^2 : \arg\min_{\mathbf{y}_i\in\Phi_{\mathrm{b}}} \|\mathbf{x}-\mathbf{y}_i\| = \arg\min_{\mathbf{y}_i\in\Phi_{\mathrm{b}}} \|\mathbf{y}_i\|\right\}$. Owing to Ext-Slivnyak theorem (Lemma 1), the load on the tagged BS consists of users of an independent copy of PLP-MCP falling in the tagged cell, plus a set of additional users falling on a part of the tagged line inside the tagged cell. As mentioned earlier, the tagged line or the road is the line on which the typical vehicle lies. The part of the tagged line falling inside the tagged cell is termed the *tagged chord* C_{o} *i.e.* $\mathsf{C}_{\mathrm{o}} = \ell_{\mathrm{o}} \cap \mathsf{V}_{\mathrm{o}}$. The tagged chord can also be defined as the chord of the tagged cell passing through the origin. Since the tagged chord's length C_{o} plays an important role in the BS's load distribution, we derive its distribution $f'_{C_{\mathrm{o}}}(c_{\mathrm{o}})$ next. While this specific result exists in [15] within the context of the load distribution in a PLP-PPP, we derive it using a new approach that yields an easy-to-use expression that does not involve higher-order derivatives. We emphasize here that this chord length distribution is not our main contribution but just an important intermediate result that will facilitate further analysis.

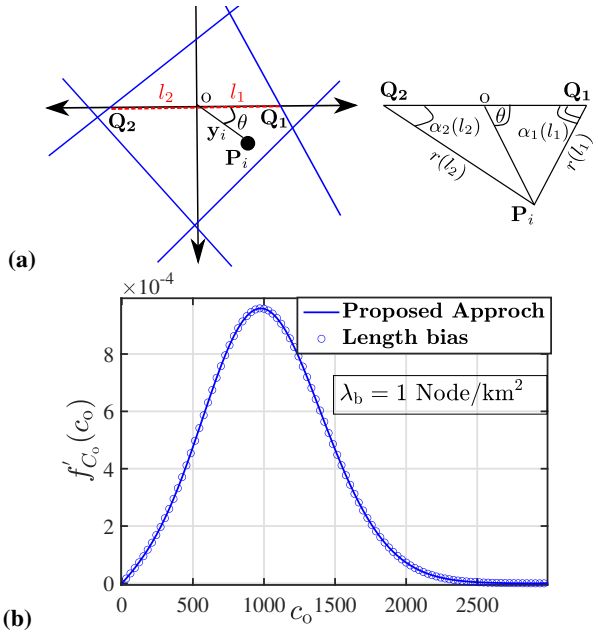

Fig. 3: (a) An illustration showing approach to find the PDF of the tagged chord length $\mathbf{Q}_1\mathbf{Q}_2$. Here, $\mathbf{P}_i$ denotes the BS. (b) The PDF obtained using the proposed method, along with the length bias result from [15].

A. Distribution of tagged chord length in the Voronoi tessellation

We adapt an approach presented in [33] to derive the joint PDF of the length of the residual chords in both sides of the origin. Using the joint PDF, we derive the PDF of the length of the tagged chord. We draw two lines from the origin in two opposite directions, (can be taken as positive and negative x-axis without loss of generality). Further, the points $\mathbf{Q}_1$ and $\mathbf{Q}_2$ where these two lines intersect X_{b}, are the two endpoints of tagged chord (as shown in Fig. 3). Let l_1 and l_2 be the distance of $\mathbf{Q}_1$ and $\mathbf{Q}_2$ from the origin. We first require the following result.

Lemma 4. *The radii* r_1 *and* r_2 *of two circles* $\mathsf{B}_2((0, l_1), r_1)$ *and* $\mathsf{B}_2((0, -l_2), r_2)$ *such that they*

intersect at a point $\mathbf{y} = y\angle\theta$ *(see Fig. 3) are given as* $r_1 = r(l_1) = \sqrt{l_1^2 + y^2 - 2l_1 y\cos\theta}$, $r_2 = r(l_2) = \sqrt{l_2^2 + y^2 + 2l_2 y\cos\theta}$ *with angles* $\alpha_1(l_1)$ *and* $\alpha_2(l_2)$ *as* $\cos\alpha_1(l_1) = \frac{l_1 - y\cos\theta}{r(l_1)}$, $\cos\alpha_2(l_2) = \frac{l_2 + y\cos\theta}{r(l_2)}$. *The area of the union of these two 2D disks is given as*

$$\mathcal{V}(l_1 + l_2, r(l_1), r(l_2)) = v_1(l_1) + v_2(l_2), \tag{31}$$

where $v_i(l_i) = r^2(l_i)\left(\pi - \alpha_i(l_i) + 0.5\sin 2\alpha_1(l_1)\right)$. *Its partial derivative are*

$$\frac{\partial \mathcal{V}}{\partial l_i} = v_i^{(1)}(l_i) = 2(l_i + y\cos\theta)(\pi - \alpha_i(l_i)) + 2y\sin\theta.$$

Using the above result, we now derive the distribution of the tagged chord length which is given in the following theorem. See Appendix D for the proof.

Theorem 5. *The joint PDF of the length of the two chord segments in the Voronoi tessellation is*

$$f_{L_1,L_2}(l_1, l_2) = 8{\lambda_\mathrm{b}}^3 \int_0^\pi \int_0^\infty e^{-\lambda_\mathrm{b}\mathcal{V}(l_1+l_2, r(l_1), r(l_2))} v_1^{(1)}(l_1) v_2^{(1)}(l_2) y \mathrm{d}y\mathrm{d}y\mathrm{d}\theta, \tag{32}$$

where $\mathcal{V}(l_1 + l_2, r(l_1), r(l_2))$ *is given in* (31). *The PDF of the length of the tagged chord in the Voronoi tessellation is*

$$f_{C_\mathrm{o}}(c_\mathrm{o}) = \int_0^{c_\mathrm{o}} f_{L_1,L_2}(c_\mathrm{o}, c_\mathrm{o} - l_2)\mathrm{d}l_2. \tag{33}$$

For completeness, note that we derived an expression for the tagged chord length in [15] using a length-biased sampling argument that provided the following expression,

$$\begin{aligned} f_{C_\mathrm{o}}(c_\mathrm{o}) &= \frac{c_\mathrm{o} f_C(c_\mathrm{o})}{\mathbb{E}[C]} = \frac{4\sqrt{\lambda_\mathrm{b}}}{\pi} c_\mathrm{o} f_C(c_\mathrm{o}) \\ &= \frac{4\sqrt{\lambda_\mathrm{b}}}{\pi} c_\mathrm{o} \frac{\pi}{2} {\lambda_\mathrm{b}}^{\frac{3}{2}} \int_0^\pi \int_0^\infty \Big[\lambda_\mathrm{b}\left(\mathcal{V}^{(1)}(c, y, r(c))\right)^2 \\ &\quad - \mathcal{V}^{(2)}(c, y, r(c))\Big] e^{-\lambda_\mathrm{b}\mathcal{V}(c,y,r(c))} y\mathrm{d}y\mathrm{d}\theta, \end{aligned}$$

which involved higher-order partial derivatives. The expression given above in Theorem 5 is slightly simpler in that sense. Further, since this specific proof idea involving the joint distribution of two chords segments has not appeared in the literature, we decided to include it here. Another advantage of the proposed approach is that it can also be extended to the case where the BS locations are distributed as a non-homogeneous PPP.

Equipped with the expressions of PDF of the tagged chord length and the number of vehicles in a set, we now analyze the vehicular communication networks in terms of the load per BS.

V. Load Distribution in a Platooned Vehicular Communication Network

In this section, we present the per-BS load distribution. The per-BS load in a communication system refers to the number of vehicles served by the BS which is defined as the number of vehicles falling inside its Voronoi region. The distribution of per-BS load is an important performance metric as it critically affects the distribution of SINR, per-user available resources and finally the rate in the following way. If a particular BS does not have any user associated with it, it may stay silent which reduces interference to the users of other BSs, and improves their SINR distribution. Conversely, as the time-frequency resources are split across the users associated with the serving BS, the load on the tagged BS reduces the resources available to the typical user. As the rate distribution depends on the per-user resources and the SINR distribution, the load on both the typical and the tagged BS plays a key role in the system's performance. Hence, we will focus on distribution of the following important metrics:

1) $S_\mathrm{m} = \Psi_\mathrm{m}(\mathsf{V}_\mathrm{t})$: Load on the typical BS.
2) $M_\mathrm{m} = \Psi_\mathrm{m}(\mathsf{V}_0)$: Load on the tagged BS.

The load distribution may help us decide the size of platoon and/or the number of vehicles in a platoon to improve performance. It may also provide us insights into the load distribution across the BSs that may help in optimizing the resource allocation, bandwidth sharing, and BS association. This is especially important in the case of PTS that may exhibit larger disparity in the per-BS load, especially for smaller values of a. Since vehicles in a platoon drive in close proximity of each other, it is highly likely that vehicles in a given platoon are served by the same BS. This may lead to situations in which one BS serves multiple platoons and hence a large number of vehicles, whereas another BS does not serve any platoon and hence no vehicle. Therefore, it is crucial to understand the nature of load distribution on BSs. As mentioned already, we will assume that the BS remains silent (and hence does not create interference) if its load is zero. We will look at an approximation ($\widetilde{S}_\mathrm{m}$ and $\widetilde{M}_\mathrm{m}$ respectively) of these variable. To approximate the load in a Voronoi cell of area $|V_\mathrm{t}|$, we will replace the cell with a 2D ball of equal area, *i.e.* the radius of this ball is $\sqrt{|V_\mathrm{t}|/\pi}$ and instead compute the load in this ball. The PDF of the radius corresponding to the typical and tagged cell is respectively given as

$$f_{R_\mathrm{t}}(r_\mathrm{t}) = 2\pi r_\mathrm{t} g_{|\mathsf{V}_\mathrm{t}|}(\pi r_\mathrm{t}^2). \tag{34}$$

$$f^\mathrm{o}_{R_\mathrm{o}}(r_\mathrm{o}) = 2\pi r_\mathrm{o} g_{|\mathsf{V}_\mathrm{o}|}(\pi r_\mathrm{o}^2) = 2\pi r_\mathrm{o}\lambda_\mathrm{b}\pi r_\mathrm{o}^2\ g_{|\mathsf{V}_\mathrm{t}|}(\pi r_\mathrm{o}^2). \tag{35}$$

A. Load distribution on the typical BS

Theorem 6. *The PGF of the load* S_m *on typical Voronoi* V_t *is (see Appendix E for proof)*

$$\mathcal{P}_{S_\mathrm{m}}(s) = \frac{\sqrt{\lambda_\mathrm{b}}}{4}\int_{z=0}^\infty \exp\Big(-\lambda_\mathrm{L} z \times \left(1 - \int_0^\infty \exp\left(g\left(s, .5c\right)\right) f_C'(c)\mathrm{d}c\right)\Big) g_{|V_\mathrm{t}|}\left(\frac{\sqrt{\lambda_\mathrm{b}}}{4}z\right)\mathrm{d}z, \tag{36}$$

where $g(s, \cdot)$ *is given in* (10). *The PMF of* S_m *is*

$$\begin{aligned} \mathbb{P}\left[S_\mathrm{m} = k\right] &= \frac{1}{k!}\left[\mathcal{P}^{(k)}_{S_\mathrm{m}}(0)\right] \\ &= \frac{\sqrt{\lambda_\mathrm{b}}}{4}\frac{1}{k!}\int_{z=0}^\infty \mathcal{P}^{(k)}_{S_\mathrm{m}|Z=z}(0) g_{|V_\mathrm{t}|}\left(\frac{\sqrt{\lambda_\mathrm{b}}}{4}z\right)\mathrm{d}z, \\ &= \frac{\sqrt{\lambda_\mathrm{b}}}{4}\frac{1}{k!}\int_0^\infty \mathcal{P}_{S_\mathrm{m}|Z=z}(0) \\ &\quad \times \mathsf{b}\left(g^{(1)}_\mathrm{m}(0), \ldots, g^{(k)}_\mathrm{m}(0)\right) g_{|V_\mathrm{t}|}\left(\sqrt{\lambda_\mathrm{b}}/4z\right)\mathrm{d}z, \end{aligned}$$

where $\mathcal{P}_{S_{\mathrm{m}}|Z=z}(0)$

$$= \exp\left(-\lambda_{\mathrm{L}} z\left(1-\int_0^{\infty}\exp\left(g\left(0,c/2\right)\right)f_C^{'}(c)\mathrm{d}c\right)\right)$$

$$g_{\mathrm{m}}^{(k)}(0) = \lambda_{\mathrm{L}} z\int_0^{\infty}\exp\left(g\left(0,c/2\right)\right) \times \mathsf{b}\left(g^{(1)}\left(0,c/2\right),\ldots,g^{(k)}\left(0,c/2\right)\right)f_C^{'}(c)\mathrm{d}c,$$

where $g(s,\cdot)$ *is given in* (10)*. Further,* $g^{(k)}(s,\cdot)$ *provided in* (11) *can be evaluated at* $s=0$*.*

Note that the mean load is equal to vehicular density times the mean size of the typical cell. Since the mean area of typical cell is $1/\lambda_{\mathrm{b}}$, we get

$$\mathbb{E}\left[S_{\mathrm{m}}\right] = \lambda_{\mathrm{m}}/\lambda_{\mathrm{b}}.$$

We can approximate S_{m} by $\widetilde{S}_{\mathrm{m}} = \Psi_{\mathrm{m}}(\mathsf{B}_2(\mathrm{o},R_{\mathrm{t}}))$. Note that conditioned on R_{t}, $\mathcal{P}_{\widetilde{S}_{\mathrm{m}}(R_{\mathrm{t}})|R_{\mathrm{t}}=r_{\mathrm{t}}}(s) = \mathcal{P}_{S(r_{\mathrm{t}})}(s)$. Deconditioning using the distribution of $f_{R_{\mathrm{t}}}(r_{\mathrm{t}})$, we get the following result.

Theorem 7. *The approximate PGF and PMF of the typical BS load are*

$$\mathcal{P}_{\widetilde{S}_{\mathrm{m}}}(s) = \int_{r_{\mathrm{t}}=0}^{\infty}\mathcal{P}_{S(r_{\mathrm{t}})}(s)\,f_{R_{\mathrm{t}}}(r_{\mathrm{t}})\mathrm{d}r_{\mathrm{t}} = 2\pi\int_{r_{\mathrm{t}}=0}^{\infty}\mathcal{P}_{S(r_{\mathrm{t}})}(s)\,r_{\mathrm{t}}g_{|V_{\mathrm{t}}|}(\pi r_{\mathrm{t}}^2)\mathrm{d}r_{\mathrm{t}}. \quad (37)$$

$$\mathbb{P}[\widetilde{S}_{\mathrm{m}}=k] = 2\pi\int_{r_{\mathrm{t}}=0}^{\infty}\mathbb{P}\left[S(r_{\mathrm{t}})=k\right]r_{\mathrm{t}}g_{|V_{\mathrm{t}}|}(\pi r_{\mathrm{t}}^2)\mathrm{d}r_{\mathrm{t}}, \quad (38)$$

where $\mathcal{P}_{S(\cdot)}(\cdot)$*, and* $\mathbb{P}\left[S(r_{\mathrm{t}})=k\right]$ *are given in Theorem 3 and* (17)*, respectively. The PDF* $g_{|V_{\mathrm{t}}|}(\cdot)$ *is given in* (29)*.*

Corollary 7.1. *The mean of* $\widetilde{S}_{\mathrm{m}}$ *is* $\mathbb{E}[\widetilde{S}_{\mathrm{m}}] = \lambda_{\mathrm{m}}\pi\mathbb{E}\left[r_{\mathrm{t}}^2\right] = \lambda_{\mathrm{m}}/\lambda_{\mathrm{b}}$*, where* $\mathbb{E}\left[r_{\mathrm{t}}^2\right] = \frac{1}{\pi\lambda_{\mathrm{b}}}$*. Similarly, to find the variance of* $\widetilde{S}_{\mathrm{m}}$*, we need the second derivative of PGF conditioned on* $s=1$ *which is given as*

$$\lim_{s\to 1}\mathcal{P}^{(2)}_{\widetilde{S}_{\mathrm{m}}}(s) = \int_{r=0}^{\infty}\left((F^1_{\mathrm{m}}(r))^2+F^2_{\mathrm{m}}(r)\right)f_{R_{\mathrm{t}}}(r)\mathrm{d}r$$

$$F^1_{\mathrm{m}}(r) = 2\pi\lambda_{\mathrm{L}}\int_{t=0}^{r}\frac{\kappa(t,1)t\mathrm{d}t}{\sqrt{r^2-t^2}},$$

$$F^2_{\mathrm{m}}(r) = 2\pi\lambda_{\mathrm{L}}\int_{t=0}^{r}\frac{\left(\kappa^2(t,1)+\kappa(t,2)\right)t\mathrm{d}t}{\sqrt{r^2-t^2}},$$

where $\kappa(t,k)$ *is given in* (12)*. Using the second derivative, mean and variance equation present in* (15)*, we get the variance of* $\widetilde{S}_{\mathrm{m}}$*.*

Corollary 7.2. *The active probability (or the on probability) of the typical BS is given as*

$$p_{\mathrm{on}} = 1-\mathbb{P}\left[S_{\mathrm{m}}=0\right] = 1-2\pi\int_{r_{\mathrm{t}}=0}^{\infty}\mathbb{P}\left[S(r_{\mathrm{t}})=0\right]r_{\mathrm{t}}g_{|V_{\mathrm{t}}|}(\pi r_{\mathrm{t}}^2)\mathrm{d}r_{\mathrm{t}}$$

with

$$\mathbb{P}\left[S(r_t)=0\right] = \exp\left(-2\pi\lambda_{\mathrm{L}}\left(r-\int_0^{r}\frac{\exp\left(g\left(0,t\right)\right)t}{\sqrt{r^2-t^2}}\mathrm{d}t\right)\right).$$

The off probability $p_{\mathrm{off}} = 1-p_{\mathrm{on}}$*.*

B. Load distribution on the tagged BS

In this section, we derive the approximate additional load $\widetilde{M}_{\mathrm{m}}$ on the tagged cell. Unlike Theorem 6, we will directly present the approximate load for the tagged cell. Here, the load $\widetilde{M}_{\mathrm{m}}$ is equal to the sum of the number of vehicles on the tagged chord (of length C_{o}) and the number of vehicles falling inside a ball of radius R_{o}. From Lemma 1,

$$\widetilde{M}_{\mathrm{m}} \overset{(d)}{=} \Psi^{\prime}_{\mathrm{m}}(\mathsf{B}_2(\mathrm{o},R_{\mathrm{o}})) + \Psi^{\prime}_{\ell_{\mathrm{o}}}(\mathsf{C}_{\mathrm{o}}) + \Omega^{\prime}_{\boldsymbol{x}_{\mathrm{o}}}(\mathsf{C}_{\mathrm{o}})$$

where $\cdot^{\prime}$ denotes the independent unconditional instances of the processes. Note that the total load counting the typical vehicle on tagged cell is $\widetilde{M}_{\mathrm{m}}+1$.

Theorem 8. *The PGF* $\mathcal{P}_{\widetilde{M}_{\mathrm{m}}}(s)$ *for the* $\widetilde{M}_{\mathrm{m}}$ *excluding the typical vehicle is*

$$\mathcal{P}_{\widetilde{M}_{\mathrm{m}}}(s) = \int_{c_{\mathrm{o}}=0}^{\infty}\int_{r_{\mathrm{o}}=0}^{\infty}\mathcal{P}_{\widetilde{M}_{\mathrm{m}}|R_{\mathrm{o}},C_{\mathrm{o}}}(s,r_{\mathrm{o}},c_{\mathrm{o}})\times f^{\mathrm{o}}_{R_{\mathrm{o}}}(r_{\mathrm{o}})f^{'}_{C_{\mathrm{o}}}(c_{\mathrm{o}})\mathrm{d}r_{\mathrm{o}}\mathrm{d}c_{\mathrm{o}}, \quad (39)$$

where,

$$\mathcal{P}_{\widetilde{M}_{\mathrm{m}}|R_{\mathrm{o}},C_{\mathrm{o}}}(s,r_{\mathrm{o}},c_{\mathrm{o}}) = \mathcal{P}_{N_{\ell_{\mathrm{o}}}}\left(s,\frac{c_{\mathrm{o}}}{2}\right)\mathcal{P}_{S(r_{\mathrm{o}})}(s) \int_{x_{\mathrm{o}}=-a}^{a}\int_{x_c=-\frac{c_{\mathrm{o}}}{2}}^{\frac{c_{\mathrm{o}}}{2}}\frac{e^{(s-1)\lambda_{\mathrm{d}}\mathcal{A}_1\left(\frac{c_{\mathrm{o}}}{2},a,|x_c-x_{\mathrm{o}}|\right)}}{c_{\mathrm{o}}2a}\mathrm{d}x_c\mathrm{d}x_{\mathrm{o}},$$

where, $\mathcal{P}_{N_{\ell_{\mathrm{o}}}}\left(s,\frac{c_{\mathrm{o}}}{2}\right)$ *and* $\mathcal{P}_{S(\cdot)}(s)$ *is provided in* (9) *and* (16)*.*

Proof. See Appendix F. □

Lemma 5. *The PMF of* $\widetilde{M}_{\mathrm{m}}$ *is given as* $\mathbb{P}\left[\widetilde{M}_{\mathrm{m}}=n\right]$

$$= \frac{1}{n!}\left[\int_{c_{\mathrm{o}}=0}^{\infty}\int_{r_{\mathrm{o}}=0}^{\infty}\sum_{k_1+k_2+k_3=n}\left[\binom{n}{k_1,k_2,k_3}\prod_{1\le t\le 3}h_t^{(k_t)}(0)\right] f^{\mathrm{o}}_{R_{\mathrm{o}}}(r_{\mathrm{o}})f^{'}_{C_{\mathrm{o}}}(c_{\mathrm{o}})\mathrm{d}r_{\mathrm{o}}\mathrm{d}c_{\mathrm{o}}\right],$$

where $h_1^{(k)}(0,r_{\mathrm{o}}) = \mathcal{P}_S^{(k)}(0,r_{\mathrm{o}})$ *is obtained in* (24) *and*

$$h_2^{(k)}\left(0,c_{\mathrm{o}}/2\right) = e^{g(0,c_{\mathrm{o}}/2)}\mathsf{b}\left(g^{(1)}\left(0,c_{\mathrm{o}}/2\right),\ldots,g^{(k)}\left(0,c_{\mathrm{o}}/2\right)\right),$$

$$h_3^{(k)}\left(0,c_{\mathrm{o}}/2\right) = \frac{1}{ac_{\mathrm{o}}}\int_{x_{\mathrm{o}}=0}^{a}\int_{x_c=-\frac{c_{\mathrm{o}}}{2}}^{\frac{c_{\mathrm{o}}}{2}}\left(\lambda_{\mathrm{d}}\mathcal{A}_1\left(c_{\mathrm{o}}/2,a,|x_c-x_{\mathrm{o}}|\right)\right)^k e^{(s-1)\lambda_{\mathrm{d}}\mathcal{A}_1(c_{\mathrm{o}}/2,a,|x_c-x_{\mathrm{o}}|)}\mathrm{d}x_c\mathrm{d}x_{\mathrm{o}},$$

and $g(0,\cdot)$ *is given in* (10)*,* $g^{(k)}(0,\cdot)$ *is given in* (11)*.*

As the conditional PGF $\mathcal{P}_{\widetilde{M}_{\mathrm{m}}|R_{\mathrm{o}},C_{\mathrm{o}}}(s,r_{\mathrm{o}},c_{\mathrm{o}})$ is a product of three PGFs, the mean and variance of $\widetilde{M}_{\mathrm{m}}$ can be written as summation of the mean and variance of the three individual RVs.

Corollary 8.1. *The mean of* $\widetilde{M}_{\mathrm{m}}$ *conditioned on* C_{o} *is*

$$\mathbb{E}\left[\widetilde{M}_{\mathrm{m}}|C_{\mathrm{o}}=c_{\mathrm{o}}\right] = 1.28\lambda_{\mathrm{m}}/\lambda_{\mathrm{b}} + m\lambda_{\mathrm{P}}c_{\mathrm{o}} + \frac{1}{2ac_{\mathrm{o}}}\int_{x_{\mathrm{o}}=-a}^{a}\int_{x_c=-\frac{c_{\mathrm{o}}}{2}}^{\frac{c_{\mathrm{o}}}{2}}\lambda_{\mathrm{d}}\mathcal{A}_1\left(\frac{c_{\mathrm{o}}}{2},a,|x_c-x_{\mathrm{o}}|\right)\mathrm{d}x_c\mathrm{d}x_{\mathrm{o}}.$$

We can further decondition using the PDF of C_{o} *as given in* (33)*. Similar to the variance of* $\widetilde{S}_{\mathrm{m}}$*, we first find the second derivative of the PGF of* $\widetilde{M}_{\mathrm{m}}$ *and then using the variance equation present in* (15)*, we find the variance of* $\widetilde{M}_{\mathrm{m}}$*.*

C. Load Distribution for the vehicular traffic under N-PTS

Since this paper also provides a comparative analysis of PTS with N-PTS, we also provide the load distribution for a vehicular communication network with N-PTS for completeness. We use the PGFs for load on the typical and the tagged cell presented in [34] to derive the mean and the variance of load. Here, the vehicles on each road form an independent 1D PPP with density λ. Hence, the overall vehicular traffic $\Psi_{\rm p}$ formed by taking the union of all the vehicles on all roads is a PLP-PPP, as discussed earlier already. Its density is $\lambda_{\rm i} = \pi\lambda_{\rm L}\lambda$. Let $\mu_{\rm p}$ denote the per-road vehicular density *i.e.* $\mu_{\rm p} = \lambda$. The mean approximate load on the typical and tagged BS in vehicular traffic under N-PTS is given as follows.

Corollary 8.2. *The mean and variance of the approximate load $\widetilde{S}_{\rm p}$ on the typical BS is*

$$\mathbb{E}\left[\widetilde{S}_{\rm p}\right] = \lambda_{\rm i}\pi\mathbb{E}\left[r_{\rm t}^2\right] = \frac{\lambda_{\rm i}}{\lambda_{\rm b}},$$

$$\mathrm{Var}\left[\widetilde{S}_{\rm p}\right] = (\lambda_{\rm i}\pi)^2\,\mathbb{E}\left[r_{\rm t}^4\right] + \frac{16}{3}\pi\lambda_{\rm L}\lambda^2\mathbb{E}\left[r_{\rm t}^3\right] + \frac{\lambda_{\rm i}}{\lambda_{\rm b}} - \left(\frac{\lambda_{\rm i}}{\lambda_{\rm b}}\right)^2,$$

where $\lambda_{\rm i} = \pi\lambda_{\rm L}\lambda$, $\mathbb{E}\left[r_{\rm t}^2\right] = \dfrac{1}{\pi\lambda_{\rm b}}$,

and $\mathbb{E}\left[r_{\rm t}^3\right] = \displaystyle\int_0^\infty r_{\rm t}^3 f_{R_{\rm t}}(r_{\rm t})\mathrm{d}r_{\rm t} = \frac{\Gamma\left((c_1+1)/a_1\right)}{b_1^{\frac{3}{2a_1}}(\pi\lambda_{\rm b})^{3/2}\Gamma\left(c_1/a_1\right)}.$

Corollary 8.3. *The mean of the approximate load $\widetilde{M}_{\rm p}$ on the tagged BS is given as*

$$\mathbb{E}\left[\widetilde{M}_{\rm p}\right] = \mathbb{E}\left[\mathbb{E}\left[\widetilde{M}_{\rm p}|C_{\rm o} = c_{\rm o}\right]\right] = \lambda_{\rm i}\pi\mathbb{E}\left[r_{\rm o}^2\right] + \lambda\mathbb{E}\left[C_{\rm o}\right].$$

Similarly, we can find the variance of $\widetilde{M}_{\rm p}$.

VI. Rate Coverage in a Platooned Vehicular Communication Network

The rate coverage is defined as the probability that the rate achievable by the typical user is greater than a certain threshold *i.e.* $\mathrm{r_c}(\tau) = \mathbb{P}(\mathcal{R} > \tau)$. Assuming that the available bandwidth B is equally shared by all user associated with the tagged BS, the achievable rate of typical receiver is given by

$$\mathcal{R} = B/(1+\widetilde{M}_{\rm m})\log_2\left(1+\mathtt{SIR}\right),$$

where $\widetilde{M}_{(\cdot)}$ is the load on the tagged BS. Also note that the SIR depends on the active BS density which is further dependent on the load distribution on the typical cell. Hence, it is evident that the rate coverage depends on the distributions of the user load on both the typical and the tagged BS. Hence, the rate coverage is

$$\begin{aligned}\mathrm{r_c}(\tau) &= \mathbb{P}\left(B/(1+\widetilde{M}_{\rm m})\log_2\left(1+\mathtt{SIR}\right) > \tau\right)\\ &= \sum_{k=0}^{\infty}\mathbb{P}(\widetilde{M}_{\rm m}=k)\mathbb{P}\left(\mathtt{SIR} > 2^{\frac{(k+1)\tau}{B}} - 1\right). \qquad (40)\end{aligned}$$

Here, $\mathbb{P}\left(\mathtt{SIR} > \tau\right)$ is the coverage probability of the typical user of a cellular network. For the channel and SIR model considered in (27), the coverage is given as [27], [29],

$$\begin{aligned}&\mathbb{P}(\mathtt{SIR} > \tau)\\ &= 2\pi\lambda_{\rm b}\int_0^\infty r\exp\left(-\lambda_{\rm b}\pi r^2 - {\rm p_{on}}\int_r^\infty \frac{2\pi\lambda_{\rm b}\tau y\mathrm{d}y}{\tau+(\frac{y}{r})^\alpha}\right)\mathrm{d}r\\ &= \int_0^\infty \exp\left(-v - {\rm p_{on}}\int_v^\infty \frac{\mathrm{d}u}{1+(\frac{u}{v})^{\frac{\alpha}{2}}\tau^{-1}}\right)\mathrm{d}v\\ &= \int_0^\infty \exp\left(-v\left(1+{\rm p_{on}}\int_1^\infty \frac{\mathrm{d}t}{1+t^{\alpha/2}\tau^{-1}}\right)\right)\mathrm{d}v\\ &= \frac{1}{1+{\rm p_{on}}\int_1^\infty \frac{\mathrm{d}t}{1+t^{\alpha/2}\tau^{-1}}},\end{aligned}$$

where the first two steps are due to the substitutions $\pi\lambda_{\rm b}y^2 = u$ and $u = vt$. Using (40), we get the following result.

Theorem 9. *The rate coverage of the typical vehicular user in a vehicular communication network with platooned vehicles is*

$$\mathrm{r_c}(\tau) = \sum_{k=0}^{\infty}\mathbb{P}\left[\widetilde{M}_{\rm m}=k\right]\left(1+{\rm p_{on}}\int_1^\infty \frac{\mathrm{d}t}{1+t^{\alpha/2}\gamma_k^{-1}}\right)^{-1}, \quad (41)$$

where $\gamma_k = \left(2^{\frac{(k+1)\tau}{B}} - 1\right)$ *and* ${\rm p_{on}}$ *is given in Corollary 7.2.*

Note that the rate coverage for a typical user in N-PTS can also be computed using (41) by replacing $\widetilde{M}_{\rm m}$ and $\widetilde{S}_{\rm m}$ with $\widetilde{M}_{\rm p}$ and $\widetilde{S}_{\rm p}$, respectively.

VII. Numerical Results

In this section, we first present numerical results using the derived expressions. We will first verify the accuracy of the PMFs of $\widetilde{S}_{\rm m}$ and $\widetilde{M}_{\rm m}$ by comparing them with the exact simulation results. We also discuss the impact of various parameters on the load distribution. After that, we will present a comparative analysis between PTS and N-PTS in terms of the energy efficiency, load imbalance and their impact on the rate coverage. Since the locations of vehicles are independent of each other because of the underlying PPP model, it is possible that the two proximate vehicles might come arbitrarily close to each other. Hence it is desirable to have a guard distance between the vehicles to improve traffic safety. One way to implement this restriction in the model is to remove those vehicles in PLP-MCP that are closer than guard distance from their neighboring vehicles. Unfortunately, the resulting process will become intractable but can be approximated using a PLP-MCP process with reduced vehicular density to compensate for the removed vehicles. Another way is to spread the closely located vehicles over multiple lanes. In that case, PLP-MCP models the projection of all vehicles onto a single line. Since lanes are close to each other, it does not affect the load or rate distribution. In all our numerical results, we use the following parameters unless stated otherwise. The road density $\lambda_{\rm L} = 5/\pi$ km^{-1}, $\lambda_{\rm P} = 1$ platoons/km $a = 250$ m. For fair comparison we have taken λ in N-PTS such that the total vehicular density $\lambda_{\rm i}$ in N-PTS is equal to $\lambda_{\rm m}$.

A. Validation

To test the accuracy of the derived distributions of the approximate load $\widetilde{S}_{\rm m}$ and $\widetilde{M}_{\rm m}$, we evaluate the Bhattacharyya coefficient (BC) [35] between the PMFs of the approximate

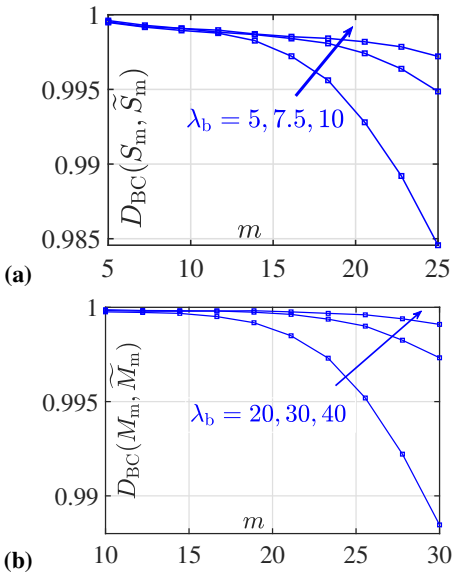

Fig. 4: The BC for (a) the typical $D_{\mathrm{BC}}(S_{\mathrm{m}}, \widetilde{S}_{\mathrm{m}})$ and (b) the tagged load $D_{\mathrm{BC}}(M_{\mathrm{m}}, \widetilde{M}_{\mathrm{m}})$ for various values of m and λ_{b}. Here, $\lambda_{\mathrm{L}} = 5/\pi$ km^{-1} , $\lambda_{\mathrm{P}} = 1$ platoons/km $a = 250$ m. A value close to 1 implies that the approximation is accurate.

load and the respective exact PMFs obtained using simulations. Note that for any two PMFs $p(\omega)$ and $q(\omega)$, the BC is defined as $D_{\mathrm{BC}}(p, q) = \sum \sqrt{p(x)q(x)}$. The BC $D_{\mathrm{BC}}(p, q)$, lies between 0 to 1, and a value close to 1 indicates good approximation. Fig. 4 presents the BC for the load on the typical $\left(D_{\mathrm{BC}}(S_{\mathrm{m}}, \widetilde{S}_{\mathrm{m}})\right)$ and the tagged cell $\left(D_{\mathrm{BC}}(M_{\mathrm{m}}, \widetilde{M}_{\mathrm{m}})\right)$. From this result, we notice that the approximation is remarkably close to the true result. The approximation improves further with decrease in platoon size m and increase in the BS density.

B. Mean and variance of the load on the typical cell

Fig. 5(a) shows the mean and variance for the approximate load on the typical cell with respect to per-road vehicular density $\mu_{\mathrm{m}} = m\lambda_{\mathrm{P}}$ for different values of the platoon radius a. From Corollary 7.1, the mean load on the typical cell depends linearly on density $\lambda_{\mathrm{m}} = \mu_{\mathrm{m}}\lambda_{\mathrm{L}}\pi$ but does not depend on a. This is also evident from the numerical results. It can be observed further that the variance grows quadratically with μ_{m} which is consistent with (20). For small a, vehicles are concentrated close to the platoon centers because of which all the vehicles of a given platoon will very likely contribute to the load of a single BS. However, as we increase a, vehicles are more spread out, which decreases the variance of load on the typical BS. We also present the respective metrics for N-PTS. Here, we keep $\mu_{\mathrm{p}} = \mu_{\mathrm{m}}$ such that the mean load will be the same for N-PTS and PTS. Further, the variance for the PTS case is higher than N-PTS, and it becomes equal to N-PTS for very large a. This convergence is due to the fact that the MCP$(\lambda_{\mathrm{P}}, m, a)$ converges to PPP $(m\lambda_{\mathrm{P}})$, as $a \to \infty$ [36].

C. Mean and variance of the load on the tagged cell

Fig. 5(b) presents the mean and variance for the approximate load on the tagged cell with respect to per-road vehicular

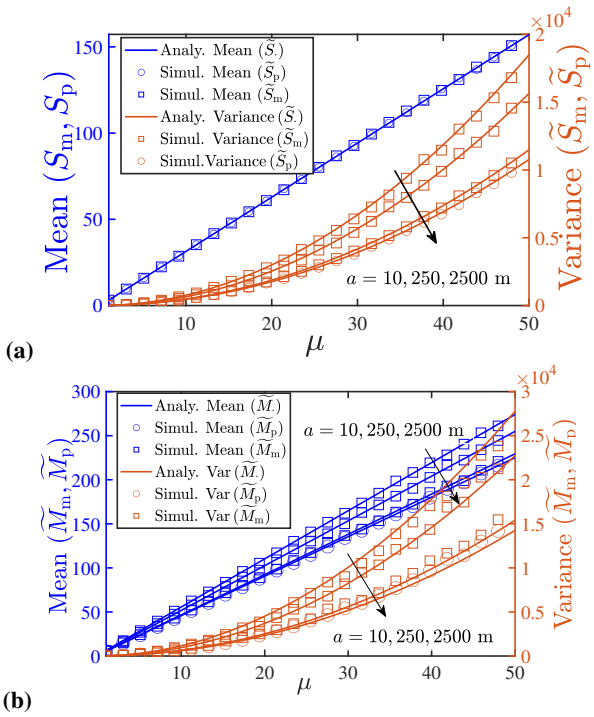

Fig. 5: The mean and variance of the load on (a) typical ($\widetilde{S}_{\mathrm{m}}$, $\widetilde{S}_{\mathrm{p}}$) and (b) tagged ($\widetilde{M}_{\mathrm{m}}$, $\widetilde{M}_{\mathrm{p}}$) cell with varying per-road vehicular density $\mu_{\mathrm{m}} = \mu_{\mathrm{p}} = \mu$. Here, for N-PTS, λ is varied as $\lambda = \mu$ per km, while for PTS, m is varied as $m = \mu/\lambda_{\mathrm{P}}$, while keeping $\lambda_{\mathrm{P}} = 1$ platoon/km. Here, $\lambda_{\mathrm{b}} = 5$ BS/km^2, $\lambda_{\mathrm{L}} = 5$ /km, and a is in meters. As a increases, the variance of $\widetilde{S}_{\mathrm{m}}$ and $\widetilde{M}_{\mathrm{m}}$ converges to variance of $\widetilde{S}_{\mathrm{p}}$ and $\widetilde{M}_{\mathrm{p}}$, respectively.

density $\mu_{\mathrm{m}} = m\lambda_{\mathrm{P}}$ for different values of the platoon radius a. Here, mean and variance of $\widetilde{M}_{\mathrm{m}}$ are higher than those of $\widetilde{M}_{\mathrm{p}}$. In PTS, the occurrence of the typical point adds points of the associated platoon in the load. Therefore, the mean and the variance of the load is higher in PTS compared to N-PTS. Further, as $a \to \infty$, the two scenarios become equivalent and the effect of the additional factor vanishes.

D. Impact of platooning on the energy efficiency of the typical cell

To further understand the typical BS load, we will evaluate two additional metrics s_{avg} and p_{u}. Here, s_{avg} is defined as the mean load of the typical BS when it is active, *i.e.*

$$s_{\mathrm{avg}} = \mathbb{E}\left[\widetilde{S}_\cdot | \widetilde{S}_\cdot > 0\right] = \mathbb{E}\left[S_\cdot\right]/p_{\mathrm{on}}.$$

The second metric p_{u} denotes the probability that the load on the typical active BS is less than the s_{avg} *i.e.*

$$p_{\mathrm{u}} = \mathbb{P}\left[\widetilde{S}_\cdot \leq s_{\mathrm{avg}} | \widetilde{S}_\cdot > 0\right].$$

Note that p_{u} represents the fraction of time the system is in a very safe operational regime. Fig 6(a) presents the off probability p_{off} of the typical BS (which also represents the fraction of BSs staying silent) in PTS and N-PTS scenario with respect to per-road vehicular density $\mu = \mu_{\mathrm{m}} = \mu_{\mathrm{p}}$. We further observe that the off probability values p_{off} obtained using the analytical expression and simulation are close. The gap occurs due to approximation of the typical cell by a disk with an equal area.

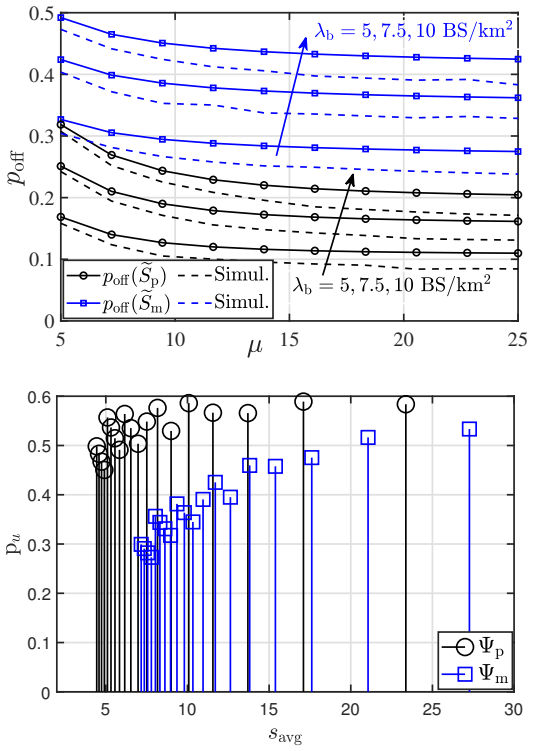

Fig. 6: (a) The variation of p_{off} with respect to per-road vehicular density $\mu_{\text{m}} = \mu_{\text{p}} = \mu$ for PTS and N-PTS. Here, for N-PTS λ is varied as $\lambda = \mu$, and for PTS, m is varied as $m = \mu/\lambda_{\text{P}}$ while keeping $\lambda_{\text{P}} = 1$ platoon/km. The fraction of BSs being switched off is higher in PTS as compared to N-PTS, indicating a better energy efficiency. (b) Variation of p_{u} with s_{avg}. Here, $\mu = 15$ vehicles/km. N-PTS has better underload probability. Here, $a = 250$ m in PTS and λ_{b} is in per km^2.

We observe that p_{off} is higher in PTS as compared to the N-PTS indicating that the energy consumption in PTS is less than N-PTS. Fig. 6(b) shows the variation of p_{u} with active load s_{avg} by varying λ_{b} from $2 - 30$ BS/km^2 while keeping the rest of the parameters fixed. As expected, the load s_{avg} on active BSs decreases with λ_{b}. Further, s_{avg} is high in PTS due to a lower fraction of BSs staying active as compared to N-PTS. Due to relatively higher load in PTS, safe-operating probability p_{u} gets lower in PTS.

Fig. 7(a)-(c) presents variation of p_{u} with respect to BS density, active BS density and off probability for N-PTS and PTS. Here, p_{u} decreases with the densification of BSs which is intuitive. Small increments found in p_{u} at some densities are due to the discrete nature of summation in the definition of p_{u}. Elaborating further, first note that the $\widetilde{S}$ can take only integer values. When s_{avg} decreases, the number of individual PMF terms may not decrease if the change in s_{avg} is fractional. However due to a decrease in the mean, the individual PMF terms increase, resulting in a net increase in p_{u}. In Fig. 7(c), we compare p_{u} between PTS and N-PTS by equating the off probability. We can see that for the same level of off probability, p_{u} is almost the same in both the cases. In Fig. 7(c), we compare p_{u} between PTS and N-PTS by equating the active BS density. Since the active probability is significantly lower in PTS, we can observe that at the same value of $\lambda_{\text{fl}} = \lambda_{\text{b}}$, p_{u} in N-PTS is lower.

E. Load balance in the tagged cell

Note that the mean load is not the only criteria for comparing two systems. For instance, it may not be optimal from the energy utilization perspective to activate a BS to just serve a single vehicle. In order to understand the effect of load distribution, we define the following metrics: single user probability p_1, the average load on tagged cell m_{avg}, and tagged safe-operating probability p_{s}, as follows

$$p_1 = \mathbb{P}\left[\widetilde{M}. = 1\right],\ m_{\text{avg}} = \mathbb{E}\left[\widetilde{M}.\right],\ p_{\text{s}} = \mathbb{P}[\widetilde{M}. \leq m_{\text{avg}}].$$

Note that, a high p_1 represents that many BSs in the system are severely underloaded. From Fig 8(a), we can observe that p_1 in lower in PTS. This indicates that it is more likely in PTS that a BS is not wasting its power to just serve a single user. Fig 8(b) shows the variation of mean load in the tagged cell which decreases with λ_{b}. Unlike the typical cell, the mean load on the tagged cell differs in PTS and N-PTS. Fig. 8(c) shows p_{s} with respect to m_{avg} using the data obtained from Fig. 8(b). We can observe that p_{s} is higher in N-PTS for the same value of m_{avg}. Together with Fig. 5(b), which shows that the variance of the load on the tagged cell is higher in PTS, we can see that the spread of load distribution is higher in PTS. This means that the tagged BS may have to support a higher number of users in PTS compared to N-PTS.

F. Rate coverage analysis

From the results thus far, we have observed that while the PTS has a higher off probability, it also has a higher per-BS load. Hence, if the system bandwidth is enough to support the load, the PTS is expected to perform better than N-PTS in terms of rate coverage. Fig. 9(a) shows the variation of rate coverage with respect to BS density for PTS and N-PTS with equal vehicular density ($\lambda_{\text{m}} = \lambda_{\text{i}}$). As expected, the rate coverage increases with the BS density. However, at any BS density, the rate coverage in PTS and N-PTS is almost equal, which may appear counter-intuitive. However, it must be noted that the active probability is significantly lower in PTS, which means that PTS can achieve almost the same rate coverage but at a much lower active BS density. This effect can be observed in Fig. 9(b) which shows the variation of the rate coverage with respect to the active BS density for PTS and N-PTS. Here, we can observe that PTS can achieve significantly higher coverage than N-PTS. Further, the densification of BSs in PTS does not impact the power budget, but still results in an improvement in the rate coverage. To quantitatively characterize the proximity of vehicles in platooned and non-platooned vehicles, we can utilize neighbor distance (NND) of MCP and PPP given in [36] and [27]. Note that the NND of a process is defined as the distance of the closest point from the typical point of the process. Comparing the two, we can see that platooning reduces the NND and hence increases the proximity of vehicles which is useful for two important reasons. First, it improves the road capacity by accommodating more vehicles in the same spread of a road. Second, a close proximity makes V2V communication among them more efficient and reliable. For example, in vehicular applications, like sending safety messages, the SINR/SNR distributions are crucial as the goal is to quickly establish a

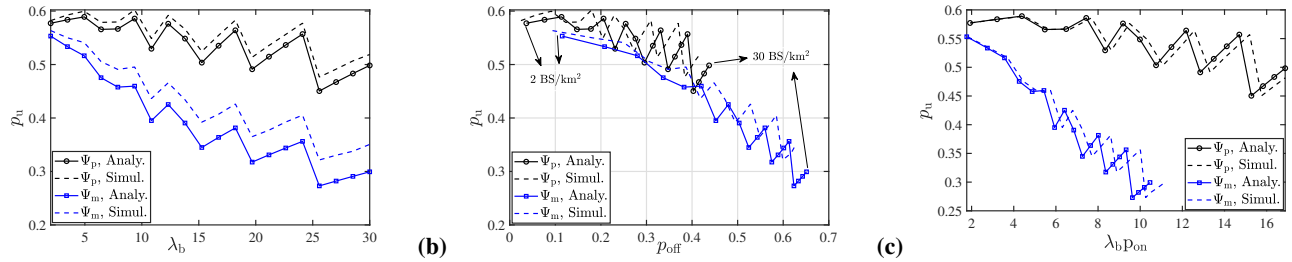

Fig. 7: Variation of p_u with respect to BS density, active BS density and off probability for N-PTS and PTS. Here, for N-PTS λ is varied as $\lambda = \mu$, and for PTS, m is varied as $m = \mu/\lambda_P$ while keeping $\lambda_P = 1$ platoon/km and $\mu = 15$ vehicles/km.

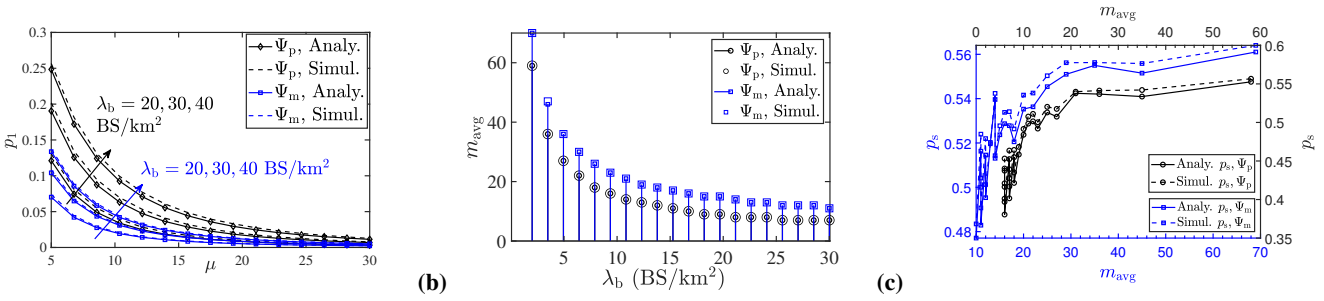

Fig. 8: (a) The variation of p_1 with respect to per-road vehicular density $\mu = \mu_m = \mu_p$, (b) mean load m_{avg} on the tagged cell with λ_b, and (c) safe-operating probability p_s with respect to m_{avg}. In (a), $\lambda_L = 2\,\text{km}^{-1}$, for (b), and (c) the parameters are $\lambda_L = 5/\pi$ km^{-1}, $\lambda = m\lambda_P = 15$ vehicles/km.

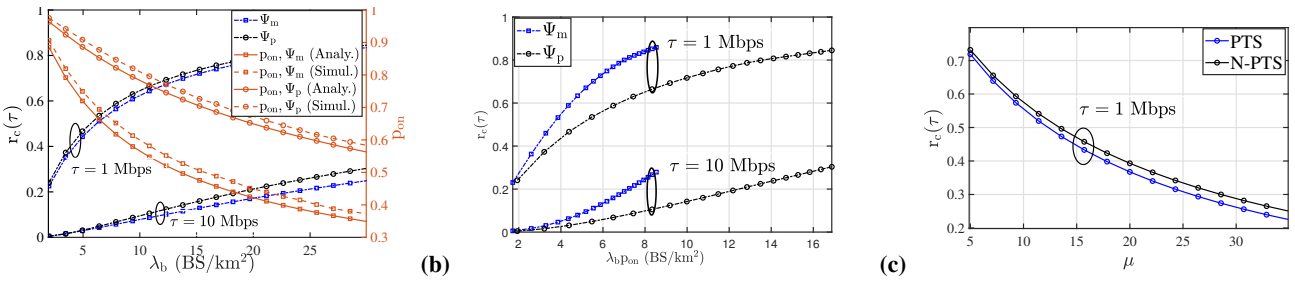

Fig. 9: Impact of the BS density and active BS density on the rate coverage and the active probability for two different values of threshold τ in PTS and N-PTS. Here, $\alpha = 3.5$, $B = 20$ MHz, and the per-road vehicular density $\lambda = m\lambda_P = 15$ vehicles/km. Hence, the mean typical load (*i.e.* B/(mean-load on typical cell)) varies between .5 MHz/users to 8 MHz/users. **(c)** shows the rate coverage for similar vehicular density on the road. We obverse that the rate coverage decreases with increase in the impact of clustering. For PTS $\lambda_P = 1$ platoon/km, $a = 250$ m, $\mu_m = \mu_p = \mu$, $B = 20$ MHz and $\lambda_b = 5$ BS/km^2.

connection to transmit a short message. Due to smaller inter-vehicle distance, it can be shown that PTS is more efficient than an NPTS. To examine the effect of clustering, we plot the rate coverage as a function of vehicular density μ while maintaining the platoon density and radius fixed as presented in Fig. 9(c). Now, for low values of μ, the clustering is minimal. Hence, the rate coverage is almost the same in PTS and N-PTS. For high values of μ, platooning causes more vehicles to be associated with the tagged BS, thereby increasing load and decreasing the rate coverage. We have shown in Fig. 9(a) that the number of active BSs in PTS is less as compared to N-PTS, which decreases interference. Hence, with less number of active BSs, we may serve each vehicle in a platoon with a rate coverage almost similar to N-PTS.

VIII. Conclusion and Future Scope

In this paper, we have developed a comprehensive approach to the modeling and analysis of platooned vehicular traffic. The approach relies on a novel point process that captures vehicular platooning by explicitly capturing three layers of randomness: (i) irregular layout of the roads by modeling them as a PLP, (ii) randomness in the placement of the platoons on each road by modeling them as a PPP, and (iii) randomness in the location of each vehicle in a platoon by modeling them collectively as an MCP. After deriving several foundational results for this *triply stochastic* process, which we called PLP-MCP, we focused explicitly on the V2I communication network for platooned traffic consisting of BSs that serve the platooned traffic. For this setting, we present several key results related to the load distributions on the typical and the tagged BSs. Using these results, we derived the per-user rate coverage of this network and provided a detailed comparative analysis of the PTS and N-PTS cases to understand the effect of vehicular platooning on the performance of the resulting vehicular network. While the rate coverage of these two cases appear similar at the first glance, we defined and studied specific distributional properties of the underlying setup to expose subtle performance trends. Our results collectively demonstrated that the rate coverage of PTS is actually higher when we account for the active BS density. Since this paper presents the very first comprehensive analytical approach to the study of platooned vehicular traffic, there are naturally many extensions possible. Most importantly, it will be interesting to consider an additional tier of roadside units, which are an important component of the emerging vehicular networks.

This will require an almost new analysis starting from the distributional results for the load on the typical and the tagged cells. It will also be useful to extend this framework to consider realistic scheduling algorithms.

APPENDIX

A. Proof of LF of Ψ_{m}: Unconditioned and under Palm

The LF of Ψ_{m} is

$$\begin{aligned}\mathcal{L}_{\Psi_{\mathrm{m}}}(v) &= \mathbb{E}_{\Psi_{\mathrm{m}}}\left[e^{\left(-\sum_{\mathbf{z}_{k,j,i}\in\Psi_{\mathrm{m}}} v(\mathbf{z}_{k,j,i})\right)}\right] \\ &\overset{(a)}{=} \mathbb{E}_{\Phi_{\mathrm{L}}}\left[\prod\nolimits_{\ell_i\in\Phi_{\mathrm{L}}} \mathbb{E}_{\Psi_{\ell_i},\ell_i}\left[\prod\nolimits_{\mathbf{z}_{k,j}\in\Psi_{\ell_i},\ell_i} e^{-v(\mathbf{z}_{k,j})}\right]\right] \\ &\overset{(b)}{=} \mathbb{E}_{\Phi_{\mathrm{L}}}\left[\prod\nolimits_{\ell_i\in\Phi_{\mathrm{L}}} \mathcal{G}_{\Psi_{\mathsf{L}(\rho_{\ell_i},\phi_{\ell_i})},\mathsf{L}(\rho_{\ell_i},\phi_{\ell_i})}(e^{-v})\right],\end{aligned}$$

where (a) is conditioned on Φ_{L}, and (b) is obtained by applying the PGFL of 1D MCP located on a line ℓ_i. Finally, applying the PGFL of the PLP, we get the LF of Ψ_{m}. For LF under Palm, we assume that the typical point of Ψ_{m} is located at the origin without loss of generality. The LF under Palm consists of the product of two terms - the LF of an independent and "unconditioned copy" of Ψ_{m}, and the LF of the MCP on the tagged line $\ell_{\mathrm{o}} = \mathsf{L}(0,\phi)$. Hence,

$$\begin{aligned}&\mathcal{L}^{!\mathrm{o}}_{\Psi_{\mathrm{m}}}(v) = \mathbb{E}^{!\mathrm{o}}\left[\exp\left(-\sum\nolimits_{\mathbf{z}_{k,j,i}\in\Psi_{\mathrm{m}}\setminus\{\mathrm{o}\}} v(\mathbf{z}_{k,j,i})\right)\right] \\ &= \mathbb{E}_{\Psi_{\mathrm{m}}}\left[\exp\left(-\sum\nolimits_{\mathbf{z}_{k,j,i}\in\Psi_{\mathrm{m}}} v(\mathbf{z}_{k,j,i})\right)\right]\mathbb{E}^{\mathrm{o}!}_{\Psi_\ell,\ell}\left[\exp\left(-v(\mathbf{z}_{k,j,0})\right)\right] \\ &\overset{(a)}{=} \mathcal{L}_{\Psi_{\mathrm{m}}}(v)\mathbb{E}^{\mathrm{o}!}_{\Psi_\ell,\ell}\left[\prod\nolimits_{\mathbf{z}_{k,j,0}\in\Psi_\ell\setminus\{\mathrm{o}\}}\exp\left(-v(\mathbf{z}_{k,j,0})\right)\right] \\ &\overset{(b)}{=} \mathcal{L}_{\Psi_{\mathrm{m}}}(v)\mathbb{E}_{\Phi}\left[\mathbb{E}^{\mathrm{o}!}_{\Psi_\ell,\ell|\phi}\left[\prod\nolimits_{\boldsymbol{z}_{k,j,0}\in\Psi_\ell\setminus\{\mathrm{o}\}}\exp\left(-v(\boldsymbol{z}_{k,j,0})\right)\right]\right] \\ &\overset{(c)}{=} \mathcal{L}_{\Psi_{\mathrm{m}}}(v)\pi^{-1}\int_0^{\pi}\mathcal{G}^{!\mathrm{o}}_{\Psi_\ell,\ell}(\exp(-v))\mathrm{d}\phi.\end{aligned}$$

Here, (a) is obtained by applying the PGFL for Ψ_{m}, (b) is due to conditioning on the orientation of tagged line $\mathsf{L}(0,\phi)$, and (c) is obtained by applying the PGFL of 1D MCP followed by deconditioning over the RV ϕ, and $\mathcal{G}^{!\mathrm{o}}_{\Psi_\ell,\ell}(\cdot)$ is given in (6).

B. Distribution of $S(r)$

Proof of Theorem 3: The number of vehicles $S(r)$ inside ball $\mathsf{B}_2(\mathrm{o},r)$ is

$$S(r) = \sum\nolimits_{\ell_i\in\Phi_{\mathrm{L}},\rho_{\ell_i}\in[-r,r]} N_{\ell_i}.$$

Recall that $N_{\ell_i} = \Psi_{\ell_i}(\mathsf{B}_2(\mathrm{o},r))$ denotes the number of vehicles on $\ell_i = \mathsf{L}(\rho_{\ell_i},\phi_{\ell_i})$ falling inside $\mathsf{B}_2(\mathrm{o},r)$. The condition indicates that the distance of the line from the origin (ρ_{ℓ_i}) needs to be inside the range $[-r,r]$ for that line to have at least one point inside $\mathsf{B}_2(\mathrm{o},r)$ [32]. Now, RVs $\{N_{\ell_1},N_{\ell_2},\ldots\}$ are independent and identically distributed (iid), hence PGF of $S(r)$ is

$$\begin{aligned}\mathcal{P}_{S(r)}(s) &= \mathbb{E}\left[\prod\nolimits_{\ell_i\in\Phi_{\mathrm{L}},\rho_{\ell_i}\in[-r,r]}\mathcal{P}_{N_{\ell_i}}(s,r)\right] \\ &= \mathbb{E}\left[\prod\nolimits_{\ell_i\in\Phi_{\mathrm{L}},\rho_{\ell_i}\in[-r,r]}\exp\left(g\left(s,\sqrt{r^2-\rho_{\ell_i}^2}\right)\right)\right],\end{aligned}$$

where the PGF of N_{ℓ_i} is given by (9). Since $\rho_{\ell_i},\phi_{\ell_i}$ are points of a PPP in $\mathbf{C}^*$, using PGFL of PPP [27], we get the desired result.

To get probability $\mathbb{P}[S(r)=k]$, we require the k-th derivative of PGF. If we define

$$f_{\mathrm{m}}(s,r) = 2\pi\lambda_{\mathrm{L}}\int_0^r\left(\exp(g(s,\sqrt{r^2-\rho^2}))-1\right)\mathrm{d}\rho,$$

PGF $\mathcal{P}_{S(r)}(s)$ takes the form of $\exp(f_{\mathrm{m}}(s,r))$. Hence, we use the Faà di Bruno's formula [37] to get (17). To get k-th derivative $f_{\mathrm{m}}^{(k)}(r)$ of $f_{\mathrm{m}}(s,r)$ at $s=0$, we need to apply the Faà di Bruno's formula one more time to get (18).

Proof of Corollary 3.2: The first derivative of $\mathcal{P}_{S(r)}(s)$ is

$$\mathcal{P}^{(1)}_{S(r)}(s) = 2\pi\lambda_{\mathrm{L}}\mathcal{P}_{S(r)}(s)\frac{\mathrm{d}}{\mathrm{d}s}\int_0^r\exp\left(g(s,\sqrt{r^2-\rho^2})\right)\mathrm{d}\rho. \quad (42)$$

Replacing $s=1$ in (42) and solving further, we get the mean of $S(r)$. Similarly, the second derivative $\mathcal{P}^{(2)}_{S(r)}(s)$ of $\mathcal{P}_{S(r)}(s)$ is

$$\begin{aligned}&= \mathcal{P}_{S(r)}(s)\left(\frac{\mathrm{d}}{\mathrm{d}s}\int_0^r 2\pi\lambda_{\mathrm{L}}\left(\exp\left(g(s,\sqrt{r^2-\rho^2})\right)\right)\mathrm{d}\rho\right)^2 \\ &+ \mathcal{P}_{S(r)}(s)\frac{\mathrm{d}^2}{\mathrm{d}s^2}\int_0^r 2\pi\lambda_{\mathrm{L}}\left(\exp\left(g(s,\sqrt{r^2-\rho^2})\right)\right)\mathrm{d}\rho \\ &= (\mathbb{E}[S(r)])^2 + 2\pi\lambda_{\mathrm{L}}\int_0^r\left[\left(g^{(1)}(1,\sqrt{r^2-\rho^2})\right)^2\right. \\ &\left.+g^{(2)}(1,\sqrt{r^2-\rho^2})\right]\mathrm{d}\rho.\end{aligned}$$

Using the second derivative of PGF of $S(r)$, we derive the variance $\mathrm{Var}(S(r))$ of $S(r)$ as

$$\begin{aligned}&\mathrm{Var}(S(r)) = \mathcal{P}^{(2)}_{S(r)}(s) + \mathbb{E}[S(r)] - (\mathbb{E}[S(r)])^2 \\ &= 2\pi\lambda_{\mathrm{L}}\int_0^r\left[\left(g^{(1)}(1,\sqrt{r^2-\rho^2})\right)^2+g^{(2)}(1,\sqrt{r^2-\rho^2})\right]\mathrm{d}\rho + \lambda_{\mathrm{m}}\pi r^2.\end{aligned} \quad (43)$$

From (11), $g^{(1)}(1,\sqrt{r^2-\rho^2})$ and $g^{(2)}(1,\sqrt{r^2-\rho^2})$ is

$$\begin{aligned}&g^{(1)}(1,\sqrt{r^2-\rho^2}) = 2\lambda_{\mathrm{P}}\left[\lambda_{\mathrm{d}}\beta(\sqrt{r^2-\rho^2})\times|\sqrt{r^2-\rho^2}-a|\right. \\ &\left.+\frac{\lambda_{\mathrm{d}}}{2}\left(\beta(\sqrt{r^2-\rho^2})\right)^2\right], \quad (44)\\ &g^{(2)}(1,\sqrt{r^2-\rho^2}) = 2\lambda_{\mathrm{P}}\left[\left(\lambda_{\mathrm{d}}\beta(\sqrt{r^2-\rho^2})\right)^2|\sqrt{r^2-\rho^2}-a|\right. \\ &\left.+\frac{\lambda_{\mathrm{d}}^2}{3}\left(\beta(\sqrt{r^2-\rho^2})\right)^3\right]. \quad (45)\end{aligned}$$

We can simplify the integrals presented in (43) based on the value of a as follows.

Case I: If $a>r$, $\beta(\sqrt{r^2-\rho^2}) = 2\sqrt{r^2-\rho^2}$. Hence,

$$\begin{aligned}&\int_0^r\left(g^{(1)}(1,\sqrt{r^2-\rho^2})\right)^2\mathrm{d}\rho = \frac{32}{3}(a\lambda_{\mathrm{P}}\lambda_{\mathrm{d}})^2r^3\int_0^r g^{(2)}(1,\sqrt{r^2-\rho^2})\mathrm{d}\rho \\ &= 8\lambda_{\mathrm{P}}\lambda_{\mathrm{d}}^2\left(\frac{2}{3}ar^3-\frac{1}{16}\pi r^4\right).\end{aligned}$$

Substituting the above values in (43), we get the variance of $S(r)$ for $a>r$.

Case II: If $a<r$, for $0<\rho<\sqrt{r^2-a^2}$, $\beta(\sqrt{r^2-\rho^2}) = 2a$, and when $\sqrt{r^2-a^2} < \rho < r$, $\beta(\sqrt{r^2-\rho^2}) = 2\sqrt{r^2-\rho^2}$. Hence,

$$\begin{aligned}&\int_0^r\left(g^{(1)}(1,\sqrt{r^2-\rho^2})\right)^2\mathrm{d}\rho = \frac{8a^2r^3}{3}, \\ &\int_0^r g^{(2)}(1,\sqrt{r^2-\rho^2})\mathrm{d}\rho = \int_0^{\sqrt{r^2-a^2}}\left(g^{(2)}(1,\sqrt{r^2-\rho^2})\right)\mathrm{d}\rho \\ &+\int_{\sqrt{r^2-a^2}}^r\left(g^{(2)}(1,\sqrt{r^2-\rho^2})\right)\mathrm{d}\rho.\end{aligned}$$

On substituting $\beta(\sqrt{r^2-a^2})$'s value and further manipulations, we get the desired result.

C. Distribution of $\widehat{S}(r)$

Proof of Theorem 4: From Theorem 1, we get

$$\begin{aligned}\widehat{S}(r) &= \Psi^{!}_{\mathrm{m}}(\mathsf{B}_2(\mathrm{o},r))|\mathrm{o}\in\Psi_{\mathrm{m}}\\ &\overset{(d)}{=} \Psi_{\mathrm{m}}(\mathsf{B}_2(\mathrm{o},r)) + \Psi_{\ell_{\mathrm{o}}}(\mathsf{B}_2(\mathrm{o},r)) + \Omega_{\boldsymbol{x}_{\mathrm{o}}}(\mathsf{B}_2(\mathrm{o},r)), \quad (46)\end{aligned}$$

where the three RVs in RHS are independent. Hence, the PGF of $\widehat{S}(r)$ is the product of 3 PGFs: the PGF of $S(r)$ $f_1(s) = \mathcal{P}_{S(r)}(s)$, the PGF of $\Psi_{\ell_{\mathrm{o}}}(\mathsf{B}_2(\mathrm{o},r))$ which is $f_2(s) = \exp(g(s,r))$ and the PGF of $\Omega_{\boldsymbol{x}_{\mathrm{o}}}(\mathsf{B}_2(\mathrm{o},r))$ which is $f_3(s) = a^{-1}\int_0^a e^{(s-1)\lambda_{\mathrm{d}}\mathcal{A}_1(r,a,x)}\mathrm{d}x$ *i.e.*

$$\mathcal{P}_{\widehat{S}(r)}(s) = f_1(s,r)f_2(s,r)f_3(s,r). \quad (47)$$

Proof of Corollary 4.1: Applying generalized Leibniz rule [38] to compute the k-th derivative of (47) and then from (13), we get (23). The derivative of $f_2^{(k)}(s,r)$ can be computed using Faà di Bruno's formula. Further,

$$\begin{aligned}f_3(s,r) &= \int_0^a a^{-1}e^{(s-1)\lambda_{\mathrm{d}}\mathcal{A}_1(r,a,x)}\mathrm{d}x, \text{ and}\\ f_3^{(k)}(s,r) &= \int_0^a \left(\lambda_{\mathrm{d}}\mathcal{A}_1(r,a,x)\right)^k a^{-1}e^{(s-1)\lambda_{\mathrm{d}}\mathcal{A}_1(r,a,x)}\mathrm{d}x.\end{aligned}$$

D. Proof of Theorem 5: Distribution of the tagged chord length

The joint CCDF of the lengths $L_1 = \mathrm{o}\mathbf{Q}_1$ and $L_2 = \mathrm{o}\mathbf{Q}_2$ can be written as

$$\overline{F}_{L_1,L_2}(l_1,l_2) = \mathbb{P}(L_1 > l_1, L_2 > l_2) = \mathbb{P}[A],$$

where event $A = \mathbb{1}(\mathbf{Q}_1, \mathbf{Q}_2$ and o belong to the same cell). If we let A_i be the event that $\mathbf{Q}_1$, $\mathbf{Q}_2$, and the origin o, all three locations lie in a single cell $V_{\mathbf{y}_i}$ of point $\mathbf{P}_i$ located at $\mathbf{y}_i$, then

$$\mathbb{1}(A) = \sum\nolimits_{\mathbf{y}_i\in\Phi_{\mathrm{b}}} \mathbb{1}(A_i).$$

Now,
$A_i = \mathbb{1}\big(\mathsf{B}_2(\mathrm{o},y_i), \mathsf{B}_2(\mathbf{Q}_1,|\mathbf{P}_i\mathbf{Q}_1|)$ and $\mathsf{B}_2(\mathbf{Q}_2,|\mathbf{P}_i\mathbf{Q}_2|)$ have no other point except $\mathbf{P}_i\big)$

$= \mathbb{1}(\mathsf{B}_2(\mathbf{Q}_1,r(l_1))$ and $\mathsf{B}_2(\mathbf{Q}_2,r(l_2))$ have no point except $\mathbf{P}_i)$.

Hence,

$$\begin{aligned}\overline{F}_{L_1,L_2}(l_1,l_2) &= \mathbb{P}[A] = \mathbb{E}\left[\sum\nolimits_{\mathbf{y}_i\in\Phi_{\mathrm{b}}}\mathbb{1}(A_i)\right]\\ &\overset{(a)}{=} \lambda_{\mathrm{b}}\int_{\mathbb{R}^2}\mathbb{P}\left(\Phi_{\mathrm{b}} \text{ has no point in } \mathsf{B}_2(\mathbf{Q}_1,r(l_1))\cup\mathsf{B}_2(\mathbf{Q}_2,r(l_2))\right)\mathrm{d}\mathbf{y}\\ &\overset{(b)}{=} \lambda_{\mathrm{b}}\int_0^{2\pi}\int_0^{\infty}\exp\left(-\lambda_{\mathrm{b}}\mathcal{V}(l_1+l_2,r(l_1),r(l_2))\right)y\mathrm{d}y\mathrm{d}\theta,\end{aligned}$$

where (a) is due to the Campbell-Mecke theorem [27] and (b) is due to conversion in polar coordinates. Now, we can compute the joint PDF $f_{L_1,L_2}(l_1,l_2)$ from the joint CDF as

$$f''_{L_1,L_2}(l_1,l_2) = \frac{\partial^2\overline{F}_{L_1,L_2}(l_1,l_2)}{\partial l_1\partial l_2},$$

which gives (32). Now, Since $C_{\mathrm{o}} = L_1 + L_2$, the PDF of C_{o} can be derived by integrating the joint PDF over the line.

E. Proof of Theorem 6: Distribution of load on the typical cell

The number of points falling in the typical cell is $S_{\mathrm{m}} = \sum_{\ell_i\in\Phi}\Psi_{\ell_i}(V_{\mathrm{t}})$. Let N be the number of chords intersecting with the typical cell V_{t}. Here, N is a Poisson RV with mean $\lambda_{\mathrm{L}}Z$, where Z is also a RV denoting the perimeter of the typical cell. Since the number of points on each chord is iid, the PGF of S_{m} conditioned on N is

$$\mathcal{P}_{S_{\mathrm{m}}|N=n}(s) = \mathbb{E}_{\Psi_{\mathrm{m}}}\left[s^{S_{\mathrm{m}}}|N=n\right] = \left[\int_0^{\infty} e^{g(s,c/2)}f'_C(c)\mathrm{d}c\right]^n.$$

Deconditioning over n, we get

$$\mathcal{P}_{S_{\mathrm{m}}|Z=z}(s) = e^{-\lambda_{\mathrm{L}}z\left(1-\int_0^{\infty}\exp\left(g\left(s,\frac{c}{2}\right)\right)f'_C(c)\mathrm{d}c\right)}. \quad (48)$$

Now, deconditioning over the distribution of Z (using the PDF of Z given in (30)), we obtain the PGF. From (13), we can compute $\mathbb{P}[S_{\mathrm{m}}=k]$ from the k-th derivative of PGF $\mathcal{P}_{S_{\mathrm{m}}}(s)$. The k-th derivative of $\mathcal{P}_{S_{\mathrm{m}}|Z}(s)$ is

$$\mathcal{P}^{(k)}_{S_{\mathrm{m}}|Z}(s) = \frac{\mathrm{d}^k}{\mathrm{d}s^k}\left(\exp(g_{\mathrm{m}}(s))\right), \quad (49)$$

where $g_{\mathrm{m}}(s) = \left(-\lambda_{\mathrm{L}}z\left(1-\int_0^{\infty}\exp\left(g\left(s,\frac{c}{2}\right)\right)f'_C(c)\mathrm{d}c\right)\right)$. As it is in the form of $f(h(s))$, we use the Faà di Bruno's formula [37] to get $\mathcal{P}^{(k)}_{S_{\mathrm{m}}|Z}(s) = \exp(g_{\mathrm{m}}(s))\,\mathsf{b}\left(g^{(1)}_{\mathrm{m}}(s),\ldots,g^{(k)}_{\mathrm{m}}(s)\right)$. To find the k-th derivative of $g_{\mathrm{m}}(s)$, we apply the Faà di Bruno's formula again and substitute $s=0$ to get the value of $g^{(k)}_{\mathrm{m}}(s)$. Now, deconditioning over Z gives the desired result.

F. Proof of Theorem 8: Approximate tagged load distribution

Note that $\widetilde{M}_{\mathrm{m}} = \Psi'_{\mathrm{m}}(\mathsf{B}_2(\mathrm{o},R_{\mathrm{o}})) + \Psi'_{\ell_{\mathrm{o}}}(\mathsf{C}_{\mathrm{o}}) + \Omega'_{\boldsymbol{x}_{\mathrm{o}}}(\mathsf{C}_{\mathrm{o}})$, where $\mathsf{C}_{\mathrm{o}} = \ell_{\mathrm{o}}\cap\mathsf{V}_{\mathrm{o}} =$ is the tagged chord and $\boldsymbol{x}_{\mathrm{o}}$ is the parent point associated with the typical point. Further note that if the tagged chord has length c_{o}, its center $\boldsymbol{x}_{c_{\mathrm{o}}}$ is distributed uniformly in $[-c_{\mathrm{o}}/2,\, c_{\mathrm{o}}/2]$. We also note that $\boldsymbol{x}_{\mathrm{o}}$ is uniformly distributed in $[-a,\, a]$ [36]. We already know the distribution of the first term. From (16), the PGF for $\Psi_{\mathrm{m}}(\mathsf{B}_2(\mathrm{o},R_{\mathrm{o}}))$ is

$$\mathcal{P}_{\Psi_{\mathrm{m}}(\mathsf{B}_2(\mathrm{o},R_{\mathrm{o}}))}(s) = \mathcal{P}_{S(R_{\mathrm{o}})}(s). \quad (50)$$

For the second term, note that $\mathsf{C}_{\mathrm{o}} = \ell_{\mathrm{o}}\cap\mathsf{V}_{\mathrm{o}} = \mathsf{B}_1(\boldsymbol{x}_{c_{\mathrm{o}}}, c_{\mathrm{o}}/2)$. Due to stationarity of $\Psi'_{\ell_{\mathrm{o}}}$ relative to the line ℓ_{o}, $\Psi'_{\ell_{\mathrm{o}}}(\mathsf{B}_1(\boldsymbol{x}_{c_{\mathrm{o}}}, c_{\mathrm{o}}/2)) = \Psi'_{\ell_{\mathrm{o}}}(\mathsf{B}_1(\mathrm{o}, c_{\mathrm{o}}/2))$. The PGF of RV $\Psi_{l_{\mathrm{o}}}(\mathsf{B}_1(\mathrm{o}, c_{\mathrm{o}}/2))$ is

$$\mathcal{P}_{\Psi_{l_{\mathrm{o}}}(\mathsf{B}_1(\mathrm{o},.5c_{\mathrm{o}}))}(s) = \mathcal{P}_{N_{\ell_{\mathrm{o}}}}(s, c_{\mathrm{o}}/2), \quad (51)$$

where $\mathcal{P}_{N_{\ell_{\mathrm{o}}}}(s, c_{\mathrm{o}}/2)$ is provided in (9). For the third term, we note that $\Omega'_{\boldsymbol{x}_{\mathrm{o}}}$ can have points only in $\mathsf{B}_1(\boldsymbol{x}_{\mathrm{o}}, a/2)$. Hence, $\Omega'_{\boldsymbol{x}_{\mathrm{o}}}(\mathsf{C}_{\mathrm{o}})$ (*i.e.* the number of points on the tagged chord due to the tagged platoon) varies depending on $\boldsymbol{x}_{\mathrm{o}}$ and $\boldsymbol{x}_{c_{\mathrm{o}}}$. It can be shown that conditioned on $\boldsymbol{x}_{c_{\mathrm{o}}}$ and $\boldsymbol{x}_{\mathrm{o}}$, $\Omega'_{\boldsymbol{x}_{\mathrm{o}}}$ is a PPP in the region $\mathsf{B}_1(\boldsymbol{x}_{\mathrm{o}}, a)\cap\mathsf{B}_1(\boldsymbol{x}_{c_{\mathrm{o}}}, c_{\mathrm{o}}/2)$ with density λ_{d}. The mean number of points in this PPP is $\lambda_{\mathrm{d}}\mathcal{A}_1(c_{\mathrm{o}}/2, a, |\boldsymbol{x}_{c_{\mathrm{o}}} - \boldsymbol{x}_{\mathrm{o}}|)$. Hence, its PGF is $\exp\left((s-1)\lambda_{\mathrm{d}}\mathcal{A}_1(c_{\mathrm{o}}/2, a, |\boldsymbol{x}_{c_{\mathrm{o}}} - \boldsymbol{x}_{\mathrm{o}}|)\right)$. Using the law of total probability, deconditioning over $\boldsymbol{x}_{c_{\mathrm{o}}}$, and $\boldsymbol{x}_{\mathrm{o}}$, the PGF of the third term is given as, $\mathcal{P}_{\Omega'_{\boldsymbol{x}_{\mathrm{o}}}(\mathsf{C}_{\mathrm{o}})}(s|C_{\mathrm{o}} = c_{\mathrm{o}}) =$

$$\int_{x_{\mathrm{o}}=-a}^{a}\int_{x_c=-c_{\mathrm{o}}/2}^{c_{\mathrm{o}}/2}\frac{e^{(s-1)\lambda_{\mathrm{d}}\mathcal{A}_1(c_{\mathrm{o}}/2,a,|x_c-x_{\mathrm{o}}|)}}{2ac_{\mathrm{o}}}\mathrm{d}x_c\mathrm{d}x_{\mathrm{o}}. \quad (52)$$

Conditioned on R_{o} and C_{o}, the three terms are independent. Therefore, the PGF of $\widetilde{M}_{\mathrm{m}}$ is the product of the PGFs of these terms, namely (50), (51) and (52). Deconditioning over R_{o} and C_{o}, we get the PGF of $\widetilde{M}_{\mathrm{m}}$.

REFERENCES

[1] S. Zeadally, M. A. Javed, and E. B. Hamida, "Vehicular communications for ITS: Standardization and challenges," *IEEE Commun. Standards Mag.*, vol. 4, no. 1, pp. 11–17, 2020.

[2] D. Jia, K. Lu, J. Wang, X. Zhang, and X. Shen, "A survey on platoon-based vehicular cyber-physical systems," *IEEE Commun. Surveys Tuts.*, vol. 18, no. 1, pp. 263–284, 2015.

[3] C. Perfecto, J. Del Ser, and M. Bennis, "Millimeter-wave V2V communications: Distributed association and beam alignment," *IEEE J. Sel. Areas Commun.*, vol. 35, no. 9, pp. 2148–2162, 2017.

[4] E. Ahmed and H. Gharavi, "Cooperative vehicular networking: A survey," *IEEE Trans. Intell. Transp. Syst.*, vol. 19, no. 3, pp. 996–1014, 2018.

[5] J. E. Siegel, D. C. Erb, and S. E. Sarma, "A survey of the connected vehicle landscape—architectures, enabling technologies, applications, and development areas," *IEEE Trans. Intell. Transp. Syst.*, vol. 19, no. 8, pp. 2391–2406, 2017.

[6] B. Blaszczyszyn, P. Mühlethaler, and Y. Toor, "Maximizing throughput of linear vehicular ad-hoc networks (VANETs)—a stochastic approach," in *Proc. European Wireless Conference*, pp. 32–36.

[7] B. Błaszczyszyn, P. Mühlethaler, and Y. Toor, "Stochastic analysis of ALOHA in vehicular ad hoc networks," *Annals of telecommunications-Annales des télécommunications*, vol. 68, no. 1, pp. 95–106, 2013.

[8] Y. Wang, K. Venugopal, A. F. Molisch, and R. W. Heath, "MmWave vehicle-to-infrastructure communication: Analysis of urban microcellular networks," *IEEE Trans. Veh. Technol.*, vol. 67, no. 8, pp. 7086–7100, 2018.

[9] ——, "Blockage and coverage analysis with mmwave cross street BSs near urban intersections," in *Proc. IEEE ICC*, 2017, pp. 1–6.

[10] F. Baccelli and S. Zuyev, "Stochastic geometry models of mobile communication networks," in *Frontiers in Queueing: Models and Applications in Science and Engineering*. CRC Press, 1996, pp. 227–243.

[11] H. S. Dhillon and V. V. Chetlur, *Poisson Line Cox Process: Foundations and Applications to Vehicular Networks*. Morgan & Claypool Publishers, 2020.

[12] S. Guha, "Cellular-assisted vehicular communications: A stochastic geometric approach," M.S. thesis, Virginia Tech, 2016.

[13] V. V. Chetlur and H. S. Dhillon, "Coverage analysis of a vehicular network modeled as Cox process driven by Poisson line process," *IEEE Trans. Wireless Commun.*, vol. 17, no. 7, pp. 4401–4416, 2018.

[14] V. V. Chetlur, S. Guha, and H. S. Dhillon, "Characterization of V2V coverage in a network of roads modeled as Poisson line process," in *Proc. IEEE ICC*, 2018, pp. 1–6.

[15] V. V. Chetlur and H. S. Dhillon, "On the load distribution of vehicular users modeled by a Poisson line Cox process," *IEEE Wireless Commun. Lett.*, vol. 9, no. 12, pp. 2121–2125, 2020.

[16] M. N. Sial, Y. Deng, J. Ahmed, A. Nallanathan, and M. Dohler, "Stochastic geometry modeling of cellular V2X communication over shared channels," *IEEE Trans. Veh. Technol*, vol. 68, no. 12, pp. 11 873–11 887, 2019.

[17] C.-S. Choi and F. Baccelli, "An analytical framework for coverage in cellular networks leveraging vehicles," *IEEE Trans. on Commun.*, vol. 66, no. 10, pp. 4950–4964, 2018.

[18] V. V. Chetlur and H. S. Dhillon, "Success probability and area spectral efficiency of a VANET modeled as a Cox process," *IEEE Wireless Commun. Lett.*, vol. 7, no. 5, pp. 856–859, 2018.

[19] ——, "Coverage and rate analysis of downlink cellular vehicle-to-everything (C-V2X) communication," *IEEE Trans. Wireless Commun.*, vol. 19, no. 3, pp. 1738–1753, 2019.

[20] C. Shao, S. Leng, Y. Zhang, A. Vinel, and M. Jonsson, "Performance analysis of connectivity probability and connectivity-aware MAC protocol design for platoon-based VANETs," *IEEE Trans. Veh. Technol*, vol. 64, no. 12, pp. 5596–09, 2015.

[21] W. Yi, Y. Liu, Y. Deng, A. Nallanathan, and R. W. Heath, "Modeling and analysis of MmWave V2X networks with vehicular platoon systems," *IEEE J. on Sel. Areas Commun.*, vol. 37, no. 12, pp. 2851–2866, 2019.

[22] T. Zeng, O. Semiari, W. Saad, and M. Bennis, "Joint communication and control for wireless autonomous vehicular platoon systems," *IEEE Trans. on Commun.*, vol. 67, no. 11, pp. 7907–7922, 2019.

[23] R. Frucht and G.-C. Rota, "Polynomios de Bell y partitiones de conjuntos finitos," *Scientia*, vol. 126, pp. 5–10, 1965.

[24] C. Gloaguen, F. Fleischer, H. Schmidt, and V. Schmidt, "Fitting of stochastic telecommunication network models via distance measures and monte–carlo tests," *Telecommunication Systems*, vol. 31, no. 4, pp. 353–377, 2006.

[25] I. W.-H. Ho, K. K. Leung, and J. W. Polak, "Stochastic model and connectivity dynamics for vanets in signalized road systems," *IEEE/ACM Transactions on Networking*, vol. 19, no. 1, pp. 195–208, 2010.

[26] V. V. Chetlur and H. S. Dhillon, "Spatial models for networks on roads: Bridging the gap between industry and academia," *IEEE Network*, vol. 36, no. 1, pp. 26–31, 2022.

[27] J. G. Andrews, A. K. Gupta, A. Alammouri, and H. S. Dhillon, *An Introduction to Cellular Network Analysis using Stochastic Geometry*. Morgan Claypool (Springer).

[28] K. Pandey, H. S. Dhillon, and A. K. Gupta, "On the contact and nearest-neighbor distance distributions for the $n-$dimensional Matérn cluster process," *IEEE Wireless Commun. Lett.*, vol. 9, no. 3, pp. 394–397, 2020.

[29] A. K. Gupta, X. Zhang, and J. G. Andrews, "Potential throughput in 3D ultradense cellular networks," in *Proc. Asilomar Conference on Signals, Systems and Computers*, 2015, pp. 1026–1030.

[30] M. Tanemura, "Statistical distributions of Poisson Voronoi cells in two and three dimensions," *Forma*, vol. 18, no. 4, pp. 221–247, 2003.

[31] J.-S. Ferenc and Z. Néda, "On the size distribution of Poisson Voronoi cells," *Physica A: Statistical Mechanics and its Applications*, vol. 385, no. 2, pp. 518–526, 2007.

[32] S. N. Chiu, D. Stoyan, W. S. Kendall, and J. Mecke, *Stochastic geometry and its applications*. John Wiley & Sons, 2013.

[33] E. Gilbert, "Random subdivisions of space into crystals," *The Annals of mathematical statistics*, vol. 33, no. 3, pp. 958–972, 1962.

[34] K. Pandey, K. R. Perumalla, A. K. Gupta, and H. S. Dhillon, "Load distribution in the typical and zero cells in a PLP-PPP vehicular communication network." [Online]. Available: https://home.iitk.ac.in/%7egkrabhi/subs/plpppp

[35] A. Bhattacharyya, "On a measure of divergence between two multinomial populations," *Sankhyā: the Indian Journal of Statistics*, pp. 401–406, 1946.

[36] K. Pandey and A. K. Gupta, "kth Distance distributions of n-dimensional Matérn cluster process," *IEEE Commun. Lett.*, vol. 25, no. 3, pp. 769–773, 2021.

[37] W. P. Johnson, "The curious history of Faà di Bruno's formula," *The American Mathematical Monthly*, vol. 109, no. 3, pp. 217–234, 2002.

[38] P. J. Olver, *Applications of Lie groups to differential equations*. Springer Science & Business Media, 2000, vol. 107.

Kaushlendra Pandey received his B.Tech. degree in Electronics and Communication Engineering from Gautam Buddh Technical University in 2010, followed by an M-Tech degree from Indian Institute of Information Technology Allahabad in 2012. After that, he worked as an assistant professor at Jaypee University of Information Technology in Solan, Himachal Pradesh, India. Currently, Kaushlendra Pandey is pursuing his Ph.D. in the modern wireless networks group within the Department of Electrical Engineering at the Indian Institute of Technology Kanpur, while also serving as an assistant professor at Central Institute of Technology in Kokrajhar. His research interests include vehicular networks, wireless sensor networks, and stochastic geometry.

Perumalla Kanaka Raju received his B.Tech. degree in Electronics and Communication Engineering from Rajiv Gandhi University of Knowledge Technologies, IIIT- RK Valley in 2019, followed by an M-Tech degree from Indian Institute of Technology Kanpur in 2021. He was recipient of DR. Vijay K. Varma Talent Award. His research interests include wireless communication, vehicular networks, stochastic geometry, and machine learning.

Abhishek K. Gupta received his B.Tech.- M.Tech dual degree in Electrical Engineering from IIT Kanpur in 2010 and PhD degree in the Department of Electrical and Computer Engineering at the University of Texas at Austin in 2016. He is currently working as an assistant professor in the Department of Electrical Engineering at Indian Institute of Technology Kanpur. He heads the modern wireless networks group at IITK. His research is in the area of stochastic geometry and modern communication systems, including 5G, mmWave, THz, vehicular, and molecular communication. He was recipient of IEI Young Engineer Award by Institute of Engineers (India) in 2021, Class of 1986 Young Faculty Fellowship by IIT Kanpur in 2022, IEEE Wireless Communication Letters Exemplary Reviewer Award in 2016, GE-FS Leadership Award by General Electric Foundation and Institute of International Education in 2009 and IITK Academic Excellence Award for four consecutive years (2006-2009). He is author of the books, An introduction to stochastic geometry (Springer Morgan-Claypool, 2023), Numerical methods using MATLAB (Springer Apress, 2014), and MATLAB by examples (Finch, 2010). Previously, he was working as Sr. standards engineer at Samsung Research America in Dallas, TX, USA. In the past, he has worked in Applied Microelectronics Circuit Corporation (Pune), Futurewei Technologies (NJ) and Nokia Networks (IL).

Harpreet S. Dhillon (Fellow, IEEE) received the B.Tech. degree in electronics and communication engineering from IIT Guwahati in 2008, the M.S. degree in electrical engineering from Virginia Tech in 2010, and the Ph.D. degree in electrical engineering from the University of Texas at Austin in 2013.

After serving as a Viterbi Postdoctoral Fellow at the University of Southern California for a year, he joined Virginia Tech in 2014, where he is currently a Professor of electrical and computer engineering, the chair of the communications area, the Associate Director of Wireless@VT research group, and the Elizabeth and James E. Turner Jr. '56 Faculty Fellow. His research interests include communication theory, wireless networks, geolocation, and stochastic geometry. He has received six best paper awards including the 2014 IEEE Leonard G. Abraham Prize, the 2015 IEEE ComSoc Young Author Best Paper Award, and the 2016 IEEE Heinrich Hertz Award. He has also received Early Achievement Awards from three IEEE ComSoc Technical Committees, namely, the Communication Theory Technical Committee (CTTC) in 2020, the Radio Communications Committee (RCC) in 2020, and the Wireless Communications Technical Committee (WTC) in 2021. He was named the 2017 Outstanding New Assistant Professor, the 2018 Steven O. Lane Junior Faculty Fellow, the 2018 College of Engineering Faculty Fellow, and the recipient of the 2020 Dean's Award for Excellence in Research by Virginia Tech. His other academic honors include the 2008 Agilent Engineering and Technology Award, the UT Austin MCD Fellowship, the 2013 UT Austin WNCG leadership award, and the inaugural IIT Guwahati Young Alumni Achiever Award 2020. He has served as the TPC Co-chair for IEEE WCNC 2022 and as a symposium TPC Co-chair for many IEEE conferences. He has also served on the Editorial boards of several IEEE journals with his current appointments being on the Executive Editorial Committee for IEEE TRANSACTIONS ON WIRELESS COMMUNICATIONS and as a Senior Editor for IEEE WIRELESS COMMUNICATIONS LETTERS. He is an IEEE Fellow, an AAIA Fellow, and a Clarivate Analytics (Web of Science) Highly Cited Researcher.